Biogeosciences, 22, 213–242, 2025
https://doi.org/10.5194/bg-22-213-2025

Biogeosciences Open Access EGU

Soil smoldering in temperate forests: a neglected contributor to fire carbon emissions revealed by atmospheric mixing ratios

Lilian Vallet[1,2], Charbel Abdallah[3], Thomas Lauvaux[3], Lilian Joly[3], Michel Ramonet[4], Philippe Ciais[4], Morgan Lopez[4], Irène Xueref-Remy[5], and Florent Mouillot[1]

[1]CEFE, Univ Montpellier, CNRS, EPHE, IRD, 1919 Route de Mende, 34293 Montpellier CEDEX 5, France
[2]French Environment and Energy Management Agency, 20 avenue du Grésillé BP 90406 49004 Angers CEDEX 01, France
[3]Groupe de Spectrométrie Moléculaire et Atmosphérique (GSMA), Université de Reims-Champagne Ardenne, UMR CNRS 7331, Reims, France
[4]Laboratoire des Sciences du Climat et de l'Environnement (LSCE), IPSL, CEA-CNRS-UVSQ, Unmagiversité Paris-Saclay, 91191 Gif-sur-Yvette CEDEX, France
[5]Institut Méditerranéen de Biodiversité et Ecologie Marine et Continentale (IMBE), Aix-Marseille Université, CNRS, Institut de Recherche pour le Développement (IRD), Avignon Université, 13290 Aix-en-Provence, France

Correspondence: Lilian Vallet (lilian.vallet@cefe.cnrs.fr, lilian.vallet@colostate.edu)

Received: 18 October 2023 – Discussion started: 21 November 2023
Revised: 25 July 2024 – Accepted: 29 July 2024 – Published: 13 January 2025

Abstract. Fire is regarded as an essential climate variable, emitting greenhouse gases in the combustion process. Current global assessments of fire emissions traditionally rely on coarse remotely sensed burned-area data, along with biome-specific combustion completeness and emission factors (EFs). However, large uncertainties persist regarding burned areas, biomass affected, and emission factors. Recent increases in resolution have improved previous estimates of burned areas and aboveground biomass while increasing the information content used to derive emission factors, complemented by airborne sensors deployed in the tropics. To date, temperate forests, characterized by a lower fire incidence and stricter aerial surveillance restrictions near wildfires, have received less attention. In this study, we leveraged the distinctive fire season of 2022, which impacted western European temperate forests, to investigate fire emissions monitored by the atmospheric tower network. We examined the role of soil smoldering combustion responsible for higher carbon emissions, locally reported by firefighters but not accounted for in temperate fire emission budgets. We assessed the CO/CO_2 ratio released by major fires in the Mediterranean, Atlantic pine, and Atlantic temperate forests of France. Our findings revealed low modified combustion efficiency (MCE) for the two Atlantic temperate regions, supporting the assumption of heavy smoldering combustion. This type of combustion was associated with specific fire characteristics, such as long-lasting thermal fire signals, and affected ecosystems encompassing needle leaf species, peatlands, and superficial lignite deposits in the soils. Thanks to high-resolution data (approximately 10 m) on burned areas, tree biomass, peatlands, and soil organic matter (SOM), we proposed a revised combustion emission framework consistent with the observed MCEs. Our estimates revealed that 6.15 Mt CO_2 (±2.65) was emitted, with belowground stock accounting for 51.75 % (±16.05). Additionally, we calculated a total emission of 1.14 Mt CO (±0.61), with 84.85 % (±3.75) originating from belowground combustion. As a result, the carbon emissions from the 2022 fires in France amounted to 7.95 MtCO_2-eq (±3.62). These values exceed by 2-fold the Global Fire Assimilation System (GFAS) estimates for the country, reaching 4.18 MtCO_2-eq (CO and CO_2). Fires represent 1.97 % (±0.89) of the country's annual carbon footprint, corresponding to a reduction of 30 % in the forest carbon sink this year. Consequently, we conclude that current European fire emission estimates should be revised to account for soil combustion in temperate forests. We also recommend the use of atmospheric mixing ratios as an effective monitoring system of prolonged soil fires that have the potential to re-ignite in the following weeks.

Published by Copernicus Publications on behalf of the European Geosciences Union.

1 Introduction

Wildfires recurrently affect European forests, particularly in the southern regions characterized by a Mediterranean climate and the northern boreal regions (European Commission, Joint Research Centre, 2023). In contrast, fire activity is significantly lower in wetter temperate and alpine forests, resulting in relatively less interest and fewer impact assessment studies (Zin et al., 2022). However, this established paradigm of wildfire distribution in Europe may undergo substantial modifications as a result of climate change (Wu et al., 2015). Climate change has the potential to intensify the already recurring fires in the Mediterranean Basin under more frequent heat waves (Ruffault et al., 2020) and reshape pyroregions (Galizia et al., 2023). In particular, the year 2022 exhibited highly distinctive fire events in the western Mediterranean Basin and experienced unusual heat waves and subsequent forest fires in the temperate forests across northern France, Germany, the Czech Republic, and the UK (Rodrigues et al., 2023). These atypical fire events could potentially serve as a preview of future fire distribution, posing a significant risk to temperate forests (Galizia et al., 2023).

However, limited information is currently available to assess the impacts of this atypical fire distribution, particularly concerning carbon emissions into the atmosphere. The gaps in our current understanding of these fires are mainly due to the rare occurrence of such fire distribution within European fire regimes, also impaired by the lack of remote-sensing measurements until recently. In a preliminary investigation of fire effects on temperate forests, Vallet et al. (2023a) focused on the 2022 fire season as a unique case study. They identified an increased loss of wood biomass in old-growth temperate forests, less affected by fires in the last decades compared to the Mediterranean forests, which are mostly affected in their early stage of forest succession as shrublands. Nevertheless, the impacts of fire on biomass combustion and the resulting carbon emission have not been assessed. Moreover, the combustion of soil, often disregarded in fire-prone Mediterranean ecosystems, remains understudied due to its thin litter layer and low soil organic content resulting from mild temperatures and high decomposition rates (Jonard et al., 2017; De Vos et al., 2015). The impact of fires on soil carbon stocks is only extensively considered in boreal forests and tropical peatlands, where fire incidence is higher (Astiani et al., 2018; Asbjornsen et al., 2005). However, temperate forests still harbor significant burnable soil carbon pools and peatlands that could contribute significantly to carbon emissions during fires (Muller, 2018; Tanneberger et al., 2017). In these ecosystems, the thick litter layer can be altered by high-temperature peaks reached during fire events, and the soil organic layer can propagate fire by so-called smoldering combustion (Watts and Kobziar, 2013). Smoldering is characterized by a slow, flameless combustion that consumes carbon and releases heat over extensive periods of time. This fire-spread mechanism can give rise to overwintering fires called "zombie fires", which may reactivate during the subsequent fire season, as observed recently in the boreal region (Irannezhad et al., 2020). Aside from fire safety considerations, these smoldering events could have significant ecological and atmospheric impacts (Watts and Kobziar, 2013) that have been overlooked in impact assessments and in fire emissions from European temperate forests (Van Wees et al., 2022; Wiedinmyer et al., 2023), mostly due to the lack of direct evidence and measurements regarding this process and its extent.

During the year 2022 in southwestern France, the region where the largest managed *Pinus pinaster* national forest of the Landes stands, firefighters consistently raised concerns about lingering soil fires that posed a potential threat for re-ignition throughout the summer and fall (Ouest-France, 2022). These fires were eventually expected to dissipate with the arrival of rainfall. However, accurately detecting and monitoring this smoldering combustion using existing Earth observation systems has proven to be challenging. Remote-sensing methods are less effective in capturing the fire effects on soils (Johnston et al., 2018) compared to the canopy (Balde et al., 2023; Fernández-Guisuraga et al., 2022), where changes in surface reflectance can be observed due to the biomass combustion during fires (Chuvieco et al., 2019) and due to the energy release detected by thermal sensors (Giglio et al., 2016; Wooster et al., 2021). Unfortunately, the information derived from aboveground assessments of fire emissions does not correlate well with soil carbon losses (Gerrand et al., 2021) due to the complex interactions between plant material and soil properties (Varner et al., 2015). Field observations of fire impacts on soils are also scarce and mainly focused on boreal peatlands (Turetsky et al., 2011a; Mack et al., 2021) or involve extensive time and effort to assess large-scale areas.

To fill this research gap on fire impacts on soil stocks and the subsequent carbon emissions across temperate European forests, we leveraged the distinctive extreme 2022 fire season in France as a case study. We hypothesized that the atmospheric signatures of trace gases could serve as a direct indicator of smoldering fires and soil organic matter (SOM) combustion. Previous investigations of smoldering combustion have shown that this partial combustion results in a high atmospheric CO/CO_2 ratio (or inversely correlated to the widely used modified combustion efficiency (MCE) index) in the absence of flaming. Various studies of smoke chemical analysis, including ground-based spectroscopy (Wooster et al., 2011), laboratory burning experiments (Hu et al., 2019), or drone/aircraft campaigns (Lee et al., 2023), have determined MCE indices ranging from 0.6 to 0.8 during smoldering combustion. Recent satellite-based studies based on Sentinel-5P (TROPOMI) retrievals have confirmed these findings by capturing CO plumes from extreme wildfires (Magro et al., 2021). Notably, Hu and Rein (2022) recently compiled a review on smoldering combustion emission factors (EFs), with MCE indices varying from

0.78–0.95 for flaming in forests to 0.7–0.90 for peatland smoldering combustion. Atmospheric mixing ratios collected by the French monitoring network, part of the Integrated Carbon Observation System (https://www.icos-cp.eu/, last access: 28 September 2023), have been used to document MCE indices at the regional scale through its wide continental network of atmospheric towers. Seasonal and interannual variations in greenhouse gas mixing ratios sampled during extreme climate events have been examined in several studies (Heiskanen et al., 2022; Ramonet et al., 2020). However, Wiggins et al. (2021) remains the only study that uses the atmospheric tower network to link low MCE values with smoldering combustion to quantify the CO emissions during the 2015 fire season in Alaska.

In our study, we utilized data from the French atmospheric tower network (https://icos-france.fr/en/, last access: 28 September 2023) collected at stations near the largest fires of 2022 in the temperate forests of the Landes and Brittany, as well as in the Mediterranean ecosystems of Provence. Our objective is twofold: firstly, to determine if variations in tower-measured MCE could be attributed to fires and to detect smoldering combustion events; secondly, to investigate whether regional variations in MCE are related to specific soil and vegetation characteristics, fire-spread features, or fire intensity indicated by remotely sensed thermal anomalies. These variables are directly associated with the fire characteristics (McArthur and Cheney, 2015), enabling the detection of smoldering combustion. Finally, we utilized our findings to provide an enhanced bottom-up fire carbon emission framework, benchmarked with the observed MCE indices, and applied it to the 2022 fire season in France. We also compared our emissions to Global Fire Assimilation System (GFAS) (Kaiser, 2023) emissions used by the Copernicus Atmosphere Monitoring Service (CAMS; Copernicus, 2023) as a reference dataset and publicly delivered in near real-time to stakeholders and society (https://ads.atmosphere.copernicus.eu/cdsapp#!/dataset/cams-global-fire-emissions-gfas?tab=overview, last access: 22 September 2023). Desservettaz et al. (2022) warned about substantial mismatches among global datasets when compared to various estimates of fire-induced CO emissions in Australia incorporating surface in situ data, ground-based total column data, and satellite-based measurements. Our study contributes to refining the global greenhouse gas budget for national fire risk assessment, regarding carbon stocks as an ecological value in the risk assessment framework developed over the European continent (Chuvieco et al., 2023).

2 Materials and methods

2.1 Study area

This study focuses on mainland France (41–52° N, 5° W–10° E). To facilitate data analysis, we divided the national territory into four regions based on forest communities and fire occurrence (Fig. 1):

- Atlantic temperate forest (sylvoecoregions A11 to A21 according to the National Forest Inventory (NFI) classification). This region is primarily characterized by agricultural land, encompassing low vegetation of pasture and cropland. However, this region comprises dense temperate forests hosting deciduous species (*Quercus petraea*, *Quercus robur*, *Fagus sylvatica*, and *Alnus glutinosa*), with coverage of approximately 11.8 %. Historically, this region experienced low fire incidence owing to its humid oceanic climate, with an annual average of 0.013 % (±0.006 %) of the forest area burned (https://bdiff.agriculture.gouv.fr/).

- Atlantic pine forest (sylvoecoregions F21 and F22 of the NFI). This region is almost exclusively covered by extensive maritime pine plantations (*Pinus pinaster*), cultivated for wood production and covering approximately 76.4 % of the region. Although this region experienced a moderate level of fire activity, with an average annual forest burning area of 0.062 % (±0.047 %), large fires were reported in 2022 (Vallet et al., 2023a).

- Mediterranean forest (sylvoecoregions J10 to K13 of the NFI). This region is characterized by low, dense forests (covering 39.8 % of the region) dominated by species typical of the Mediterranean climate (*Quercus ilex*, *Quercus pubescens*, *Quercus suber*, and *Pinus halepensis*). This region experiences a high frequency of fires, with approximately 0.25 % (±0.21 %) of the forest area burned each year.

- Other temperate forests encompassing the remaining forested land of France. This region comprises diverse temperate forest communities covering 28.3 % of the area, dominated by deciduous or coniferous species and exhibiting varying levels of management intensity. Historically, this region experienced minimal fire occurrence, with an average annual forest burning area of 0.016 % (±0.002 %)

2.2 Fire data

2.2.1 Fine-resolution fire polygons

For the fire season 2022, we delimited fire polygons using the semi-automated burned area mapping tools (BAMTs) (Bastarrika et al., 2014; Roteta et al., 2021). This method was exclusively applied to fires exceeding 30 ha and over ignitions

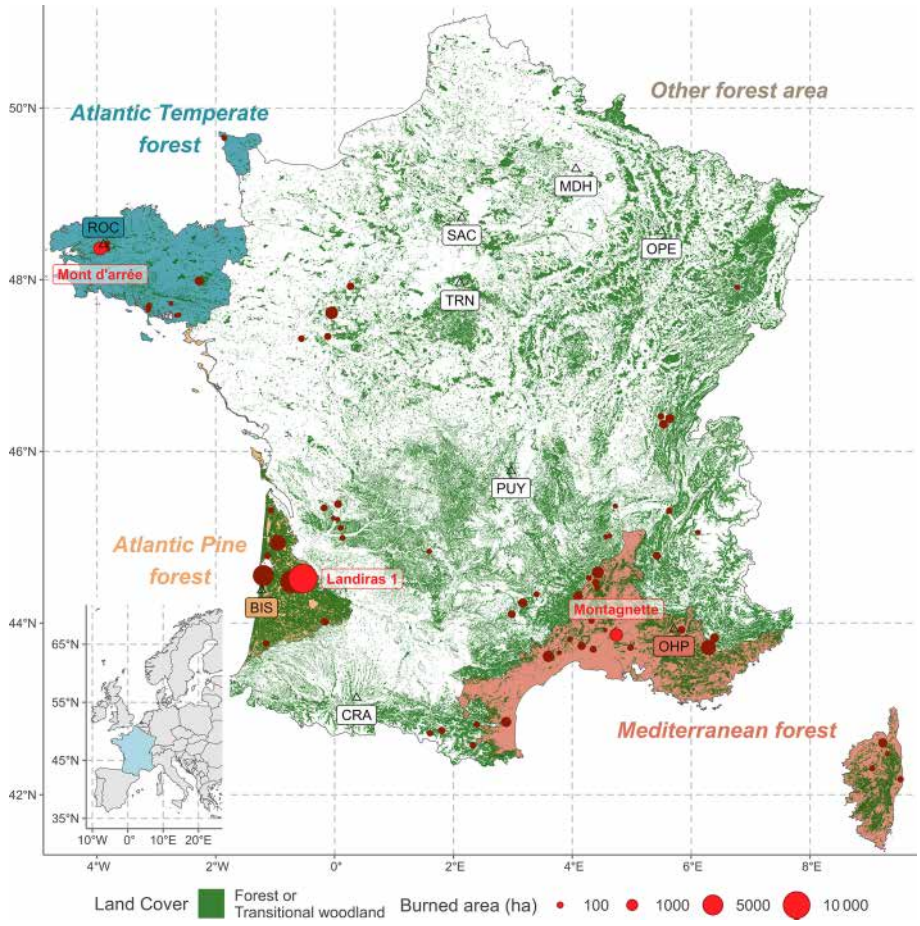

Figure 1. Map of French forests with the location of fires larger than 30 ha that occurred in the 2022 fire season. France is divided into four regions ("Atlantic Temperature forest", "Atlantic pine forest", "Mediterranean forest", and "Other forest area") according to forest type (https://inventaire-forestier.ign.fr/spip.php?article773, last access: 9 March 2023) and frequency of fire disturbance (https://bdiff.agriculture.gouv.fr/, last access: 8 March 2023). The locations of the atmospheric towers (including ROC: Roc'h Trédudon, BIS: Biscarrosse, and OHP: Observatoire de Haute-Provence) and the burned areas of the three corresponding main fires of interest are also represented ("Mont [sic] d'Arrée", "Landiras 1", and "Montagnette"; red circles).

captured by the Visible Infrared Imaging Radiometer Suite (VIIRS, on board the Suomi and NOAA-20 satellites) within wildlands (Schroeder et al., 2014). VIIRS data experience a temporal resolution of roughly 6 h and detect land surface thermal anomalies (1000 K) at 375 m resolution so that small and fast-spreading fires can be missed. However, this information has been shown to be reliable for fires above 10 ha in Mediterranean areas (Majdalani et al., 2022). BAMTs use atmospherically corrected and orthorectified images from the L2A product of ESA's Sentinel-2 mission of 2022 to derive three key spectral indices: normalized difference vegetation index (NDVI) (Rouse et al., 1974), normalized burn ratio (NBR) (Key and Benson, 1999), and NBR2 (García and Caselles, 1991). We used the VIIRS-derived fire dates to set pre- and post-burn time frames to capture the difference in these three indices between the two periods, represented in an RGB color scale. Specifically, the pre-fire period extended from the onset of the year (1 January) up to the earliest date of hotspot clusters identified by VIIRS. The post-fire period encompassed several weeks after the fire ignition and ensured a sufficient number of cloud-free satellite images. Through a visual examination of the RGB spectrum, we manually defined two sample training regions, with one being within a high signal difference and regarded as burned and the other being within a low signal difference and regarded as unburned. A random-forest (RF) classifier (Belgiu and Drăguţ, 2016) then classifies each pixel of the study area as burned or unburned according to how similar its spectral indices are to either training region. A quality assessment of the automatically processed classification was performed through visual inspection (see Vallet et al., 2023a), and training regions were fine-tuned if obvious misclassifications were detected. This key step, unavailable in current automated methods, ensures the international stan-

dards advocated by the CEOS Working Group on Calibration and Validation of remote-sensing datasets (Franquesa et al., 2020). Focusing on fires exceeding 30 ha and confined to the fire season (June to September), we identified a total of 70 fire polygons in the year 2022. These fire polygons were primarily located in forested and shrubland areas. Among these fire polygons, we studied only three of them located in the proximity of atmospheric towers for in-depth analysis of emissions, further referred to as "main fires" (description in Table 3). These three fires were the largest occurring in each region in the fire season 2022.

2.2.2 Fire intensity and fire spread

To enhance the precision of our analysis regarding fire behavior during propagation, we incorporated supplementary data, specifically surface thermal anomaly information for active fire detection. These data were gathered from Moderate Resolution Imaging Spectroradiometer (MODIS) instruments on the Terra and Aqua satellites (MCD14ML) (Giglio et al., 2016), featuring a spatial resolution of 1 km. Additionally, we harnessed Visible Infrared Imaging Radiometer Suite (VIIRS) data from the Suomi National Polar-orbiting Partnership (SNPP) and the National Oceanic and Atmospheric Administration (NOAA), offering a finer spatial resolution of 375 m (Schroeder et al., 2014). The acquisition of these datasets was facilitated through the utilization of the Fire Information for Resource Management System (FIRMS; https://firms.modaps.eosdis.nasa.gov/map/, last access: 22 March 2023). Subsequently, we executed a spatial filtration process to exclude all thermal anomalies occurring outside the confines of our designated fire patches.

The thermal anomalies derived from these datasets were instrumental in our analysis, primarily regarding assessing the intensity of fires during their propagation. We gauged this by examining the fire radiative power (FRP) values, a recognized indicator of combustion intensity (Wooster et al., 2005). Furthermore, to gain insights into the direction and daily rate of fire spread, we leveraged the temporally dated (3 to 9 h intervals) spatial locations of fire hotspots. Employing an ordinary kriging method, a geostatistical interpolation technique available through the gstat R package (Gräler et al., 2016), we used the timing (expressed in decimal days) as the target variable for interpolation, similar to previous studies (Parks, 2014; Veraverbeke et al., 2014; Scaduto et al., 2020). For each main fire, we manually fine-tuned a Gaussian or spherical function to derive the best-fitted variogram. Finally, we computed the hotspot density (number per hectare) within each fire polygon over the entire fire duration. This approach allows us to capture protracted soil and peatland fires that exhibit either a heightened hotspot density or an extended burning period (Usman et al., 2015).

2.3 Atmospheric CO / CO_2 mixing ratio analysis

In this study, we collected hourly measurements of CO and CO_2 mixing ratios derived from a subset of instrumented towers that are part of the French monitoring network (https://www.aeris-data.fr/projects/icos-service-national-dobservation-icos-france-atmosphere-sifa/, last access: 18 October 2023), a network established for monitoring atmospheric greenhouse gas variations in the atmosphere. These measurements were conducted with high-precision cavity ring-down spectroscopy (CRDS), with up to three sampling levels (Conil et al., 2019; Lelandais et al., 2022; Lopez et al., 2015; Schmidt et al., 2014). The selected stations, outlined in Table 1, include distant stations and nearby stations located within 20 km of the 2022 large fires that occurred in the Atlantic temperate forests (Brittany), Atlantic pine forests (Landes), and Mediterranean forests. Data collection for this study spanned 15 June to 1 September 2022. In the context of the Atlantic pine forest, starting on 12 July, the dominant winds were from the northeast, propelling the plume seaward. Notably, a shift in wind direction occurred on 14–15 July, with the wind veering to the north-northwest. This shift contributed to the highest CO peaks observed at the Biscarrosse (BIS) station. Subsequently, on 19 July, the wind shifted westward, transporting the plume inland and leading to elevated CO concentrations at distant stations. Similarly, in the Atlantic temperate forest (Brittany), predominant winds came from the northeast, steering the plume away from the Roc'h Trédudon (ROC) station toward the ocean. Changes in the wind direction led to intermittent CO signals at the ROC station. The only instance when the plume was transported inland occurred on 19 July.

To determine the locations of the sources corresponding to the identified CO mixing ratio anomalies observed at the atmospheric towers, we computed back-trajectories representing the different air masses sampled at the tower locations. This step was accomplished using the Hybrid Single-Particle Lagrangian Integrated Trajectory (HYSPLIT) model (Stein et al., 2015). In a backward-in-time configuration, particles were released from the receptor site and monitored over 7 d intervals. The result is a footprint matrix representing the influence of the area around the receptor on the measurements. The model spatial resolution used is $0.05° \times 0.05°$. The Global Forecast System (GFS) meteorological model (National Centers For Environmental Prediction/National Weather Service/NOAA/U.S. Department Of Commerce, 2015) provided the atmospheric conditions (wind and turbulence) to drive these particles from the receptors to the sources in the HYSPLIT simulations. The GFS outputs, featuring a horizontal resolution of $0.25° \times 0.25°$ and 3-hourly time intervals, served as the meteorological inputs. We also conducted HYSPLIT simulations in a forward-in-time configuration, releasing particles (600 per hour) from the fire locations over the fire duration from the exact burned area. In this configuration, we simulated the transport of the

Table 1. Summary of the random-forest model's performance across the atmospheric stations. The performance metrics are the coefficient of determination (R^2) and the root-mean-square error (RMSE). The tower location and height are also included.

Tower short name	Location	Height	RF performance			
			CO		CO_2	
		(m a.g.l.)	R^2	RMSE (ppb)	R^2	RMSE (ppm)
BIS	44.38° N, 1.23° W	73	0.76	9.04	0.96	1.12
CRA	43.13° N, 0.37° E	60	0.76	9.05	0.96	1.35
MDH	49.24° N, 4.06° E	48	0.74	8.43	0.89	1.56
OPE	48.56° N, 5.5° E	50	0.77	7.18	0.96	1.22
PUY	45.77° N, 2.97° E	10	0.85	6.61	0.98	0.82
ROC	48.41° N, 3.89° W	80	0.85	5.85	0.98	0.65
SAC	48.72° N, 2.14° E	100	0.79	8.62	0.96	1.34
TRN	47.96° N, 2.11° E	50	0.79	6.41	0.96	1.16

plume from the fires to the ICOS stations. By tracking the arrival times of the fire-emitted-particles within an influence region surrounding each atmospheric tower, we successfully attributed a fire source to each anomaly. These influence areas featured varying radii to account for transport uncertainties, considering that the minimum distance between the towers and the nearest fires ranged from 7 to 650 km. For towers in proximity to active fires (within 20 km), the influence radius was set at 4.5 km, corresponding to a single HYSPLIT grid cell. For more distant towers, the influence radius was extended to 25 km to account for errors associated with long-distance transport.

To quantify the excess in CO and CO_2 mixing ratios originating from the fires, we needed to determine the background concentration levels that would have been observed in the absence of fires. Due to the extensive duration of some observed fire events (> 10 h), a simple interpolation method could not be used without impacting our enhancements with variations in the background air (e.g., diurnal cycle, sea breeze periods). To determine the background flow more accurately, we trained a random-forest (RF) regression model for each gas at each station. The RF model is a non-parametric statistical method based on averaging over ensembles of multiple regression trees (Breiman, 2001). In our approach, we randomly divided the atmospheric observations into three categories: (1) the studied data, (2) the training data, and (3) the testing data. Initially, we isolated the data that were indicative of forest fire contributions to the observations. These periods were characterized by elevated CO mixing ratios and were automatically identified as outliers by Tukey's fence approach (Tukey, 1977). Subsequent manual quality checks ensured that the flagged data coincided with the active forest fire periods. The remaining data were then divided into training (70 % or approximately 1000 data points) and testing (30 % or around 400 data points) sets for each individual station. In addition to the mixing ratios, meteorological and calendar data were included as input variables for the RF models. The meteorological data encompassed the following parameters: 10 m wind speed and direction ($m\,s^{-1}$), 2 m temperature (°C), and boundary layer height (BLH) (m). These meteorological parameters were extracted from the ERA5 hourly reanalysis dataset (Hersbach et al., 2020). Time-derived variables included the hour of the day, day of the week, day of the month, and month of the year. For the RF model, the number of regression trees was set to 100.

The RF model performance was assessed using the testing data, with evaluation metrics including the coefficient of determination (R^2) and the root-mean-square error (RMSE). The model's performance scores exhibited variability across sites. On average, we achieved a correlation of 0.77 and 0.97, along with an RMSE of 7.66 and 1.12 ppm for CO and CO_2, respectively (Table 1).

The excess mixing ratios of CO and CO_2 attributable to the fires, denoted as $\Delta[CO]$ and $\Delta[CO_2]$, were calculated as the difference between the observed mixing ratios and the simulated background mixing ratios generated by our RF model. Subsequently, we computed the modified combustion efficiency (MCE), with values indicating higher levels during flaming fires combustion and lower levels during smoldering fires, according to Eq. (1) (Hao and Ward, 1993; Yokelson et al., 1996):

$$\mathrm{MCE} = \frac{\Delta[CO_2]}{\Delta[CO_2] + \Delta[CO]}. \quad (1)$$

2.4 Above- and belowground dry matter stock

To further comprehend the origin of the MCE observed at the monitoring towers, we sought to estimate the carbon pools affected by the fires, possibly contributing to the emissions of CO and CO_2. Given that our analytical framework relies on emission factors (EFs) expressed in grams of gas emitted per kilogram of dry matter (DM) consumed, we expressed these pools in units of tonnes of dry matter. The entirety of the ecosystem dry matter stock is partitioned into two distinct types: the aboveground stock (AGS) and the belowground

stock (BGS). Each of these stock types encompasses multiple pools. The AGS comprises the stem, branch, leaf, shrub, grass, and litter pools, while the BGS includes soil organic matter (SOM), peat, and lignite pools.

2.4.1 Forest stem and branch pool

Within the AGS affected by fires, the stem and branch pools are prominent components. These pools align with the woody AGB-L (aboveground biomass loss) method introduced by Vallet et al. (2023a). This method is based on two high-resolution data sources: firstly, a 10 m resolution mapping of vegetation height obtained from GEDI, Sentinel-1, and Sentinel-2 satellite images from 2020 (Schwartz et al., 2023); secondly, data indicative of forest communities and individual descriptors, sourced from the French National Forest Inventory (NFI) since 2005 (https://inventaire-forestier.ign.fr/, last access: 9 October 2023). Data supplied by the NFI within a 5 km radius of fire were used to delineate individual and population allometric relationships.

Based on the remotely sensed data on vegetation height, we estimated the biomass of a model tree within each burned pixel. Subsequently, for each pixel, we determined a tree density based on the biomass of the model tree and the density-dependent relationship derived from NFI data. After applying the AGB-L method to each 10 m burned pixel, we segregated the aboveground forest biomass into stem pools and branch pools. Deciduous branches accounted for 39 % of the aboveground biomass, while coniferous branches contributed 25 % (Loustau, 2010).

2.4.2 Shrub, grass, and litter pools

To account for the effects of the AGS on non-forest pixels (where the height is less than 3 m), we applied a fixed biomass (dry weight) density value of $10\,\mathrm{t\,DM\,ha^{-1}}$ for shrubland vegetation and $4\,\mathrm{t\,DM\,ha^{-1}}$ for herbaceous vegetation (Vallet et al., 2023a). These values are in agreement with the stocks included in the FINN carbon emission model (Wiedinmyer et al., 2023). Pixels were classified as containing shrubland vegetation based on the presence of sclerophyllous vegetation in the CORINE Land Cover (CLC) database (EEA, 2019), along with a recorded vegetation height below 3 m. Pixels not classified as forest or shrubland were regarded as grassland.

The litter pool was also incorporated into the AGS. It was derived from the GFED5 dataset, available at a resolution of 500 m by Van Wees et al. (2022). We resampled these fine litter data to a 10 m resolution using the nearest-neighbor method.

2.4.3 Forest and shrubland leaf pool

The leaf pool, representing the fraction of vegetation most completely consumed during combustion, was quantified based on a combination of satellite data and in situ measurements of leaf traits. Leaf area index (LAI) data at a resolution of 300 m were derived from the Sentinel-3 LAI product provided by the Copernicus service (Verger et al., 2014). These data were compiled over the summer period of 2022 (June to September), and the average of the non-zero values for each pixel was extracted. Specific leaf area (SLA; in $\mathrm{m^2\,kg\,DM^{-1}}$) was obtained at a resolution of 500 m from the TRY database (Moreno-Martínez et al., 2018). To calculate leaf mass, we initially conducted a nearest-neighbor resampling of LAI and SLA maps at 10 m resolution. Subsequently, the leaf pool density ($\mathrm{kg\,DM\,m^{-2}}$) was determined by dividing the LAI values ($\mathrm{m^2\,m^{-2}}$) by the SLA values ($\mathrm{m^2\,kg\,DM^{-1}}$) for each pixel. Only pixels categorized as forest or shrubland (height > 3 m) were included in this leaf pool dataset.

Consequently, the AGS is then composed of six pools: stem, branch, leaf, shrub, grass, and litter.

2.4.4 Soil organic matter (SOM) pool

The soil organic matter (SOM) is encompassed within the BGS. Data for this pool were sourced from the European Soil Data Centre (ESDAC) (Yigini and Panagos, 2016), offering carbon density values ($\mathrm{t\,C\,ha^{-1}}$) for the top 20 cm of soil at a resolution of 1000 m. To determine the pool of soil organic matter within each burned pixel, we converted these carbon values into organic matter, assuming a carbon content of 0.5 (Pribyl, 2010). These data were then resampled at 10 m resolution using the nearest-neighbor approach.

2.4.5 Other belowground pools: peatland and lignite

To investigate the sources of smoldering combustion and pyrolysis, we considered two additional pools within the BGS. Marshland areas, particularly peatland, can potentially contain huge amounts of organic matter, which is often assumed to be insignificant in temperate forest fire emissions. During the summer, waterlogged areas can become vulnerable to fire as they dry out. To account for peatland areas, we relied on the CORINE Land Cover (CLC) database (EEA, 2019). We established a fixed characterization of the peatland, assuming a depth of 2 m and a mass density of $145\,\mathrm{kg\,DM\,m^{-3}}$, as measured in France (Pilloix, 2019). We then calculated the pool mass for any point within the CLC polygon by multiplying the pixel area ($\sim 100\,\mathrm{m^2}$) by the depth and biomass density.

Lignite is a distinctive pool within the BGS found in the Landes, arising from a slow decomposition process. Historically, lignite has been utilized as an energy source in the Landes, near the city of Hostens, for its high concentration of carbon. Firefighters in this area reported high soil temperatures near the ancient mines. The lignite layer is near the surface and located beneath the organic soil. The location of the lignite area was provided by APPHIM (Apphim, 2023) around the Hostens village. The lignite mine typically has a depth ranging from 2 to 5 m, extending to 10–15 m. For our analysis, we assumed a fixed depth of 2 m (http:

//www.geocaching.com/, last access: 25 July 2023). The bulk density of brown coal is generally around 700 kg DM m^{-3} (Kopp, 2024). Accordingly, the density of the lignite pool was set at 1400 kg DM m^{-2} of burned surface. This particular pool of carbon was affected by two large fires during the 2022 fire season.

Thus, the BGS encompasses three pools: soil organic matter (SOM), peat, and lignite.

2.5 Carbon emissions

Utilizing information from fire polygons (Fig. 2, "Database") and from the estimation of AGS and BGS pools (Fig. 2, "Stock"), we estimated CO_2 and CO emissions arising from two combustion phases, namely flaming (F) and smoldering (S). This quantification was computed for each of the AGS (stem, branch, leaf, shrub, grass, and litter) and BGS (SOM, peat, and lignite) pools. Emission assessment was facilitated by accounting for two crucial factors: the combustion completeness (CC), denoting the proportion of the pool altered by combustion, and emission factors (EFs; in g $kgDM^{-1}$) for CO_2 and CO. For each individual pixel within the fire patch (p), each specific pool (P) (Table 2), and each gas (x), we calculated emission (E) using the following equation:

$$E_{Px} = M_P \cdot \mathrm{CC}_P \cdot (\mathrm{SF}_P \cdot \mathrm{EF}_{Pxs} + (1 - \mathrm{SF}_P) \cdot \mathrm{EF}_{Pf}). \quad (2)$$

- E_{Px}: emission of gas x from pool P (g)
- M_P: dry mass of pool P (kg DM)
- CC_P: combustion completeness of pool P (percentage of available pool)
- SF_P: smoldering fraction of pool P (percentage of combusted pool in smoldering phase)
- EF_{Pxs} and EF_{Pxf}: emission factors for pool P into gas x during the smoldering (s) and flaming (f) phases (g kg^{-1} DM)

To calculate the emissions of gas x (Fig. 2, "Emission") from all pools (n pools P) within each burned pixel (p), we utilized the following:

$$E_{px} = \sum_{P=1}^{n} E_{Px}. \quad (3)$$

Consequently, we were able to obtain an aggregated emission value for gas x encompassing the entire fire (A) comprising m individual pixels p, as specified in Eq. (4):

$$E_{Ax} = \sum_{p=1}^{m} E_{px}. \quad (4)$$

Table 2 provides a comprehensive summary of CC, EF, and SF for each pool, drawing from a bibliographical review of available data from global fire emission models, such as GFED (Van Wees et al., 2022) and FINN (Wiedinmyer et al., 2023), along with empirical field measurements conducted in temperate forests. Notably, in the absence of specific data synthesis for Europe, the fraction of smoldering combustion for each pool was inferred from data collected in American temperate forests (Prichard et al., 2020). We provide a range of values for combustion completeness ($\mathrm{CC}_{\min}$ and $\mathrm{CC}_{\max}$). The estimated values for combustion matter (M), emission (E), and MCE correspond to the average between the minimum and maximum estimates. The uncertainty ranges correspond to the deviation between this mean value and the limit value (minimum or maximum value having the same deviation from the mean).

To provide comparable information on our fire-level emissions and the hourly MCEs derived from measurement obtained by the atmospheric towers, we set up three distinctive stages in the fire propagation:

1. The spreading stage (SS), where the AGS constitutes the entire combustion. A total of 50 % of the AGS is affected during this phase.
2. The mixed stage (MS), characterized by ongoing aboveground flaming at the fire front while smoldering combustion consumes the wood residual and BGS over the previously burned area. This stage involves 50 % of the AGS and 25 % of the BGS.
3. The post-spreading stage (PSS), devoid of flaming but marked by continuing smoldering in the soil and wood residuals, representing the totality of emissions. Altogether, 75 % of the BGS is impacted during the post-spreading stage.

The splitting of the BGS smoldering at 75 % during the post-spreading stage and 25 % during the mixed stage relies on the flaming duration of 10 d for the BIS fire and with an extended 15 d (to be conservative) after the spreading. The mixed stage lasted 5 d, representing 25 % of the smoldering period lasting these 5 d plus the 15 d after the spreading (20 d of smoldering duration). This is a conservative value, as smoldering lasted for longer but with much less intensity. We also tested for accurate MCEs during this mixed stage (see flowchart Fig. A1) to keep this fraction.

These three stages were applied to the three main fires, calibrating the combustion completeness of each pool. More precisely, we tested different sets of CC values until the model MCEs and the tower-measured MCEs corresponded. Once the refined CC values were defined, we applied this fire model to all the fire polygons obtained in 2022. Belowground combustion (i.e., BGS combustion) was only applied to fires corresponding to selected criteria for smoldering (Fig. A1).

For comparison, we utilized the Global Fire Assimilation System (Kaiser, 2023) dataset for fire emissions (Kaiser et al., 2012). This dataset is the only one to offer near-real-time coverage extending to 2022, generating daily emissions based on MODIS MCD thermal "hotspot" anomalies and the biome-specific combustion rate (in kg DM MJ^{-1}). GFAS delivers information at a 0.1° resolution, covering burned dry

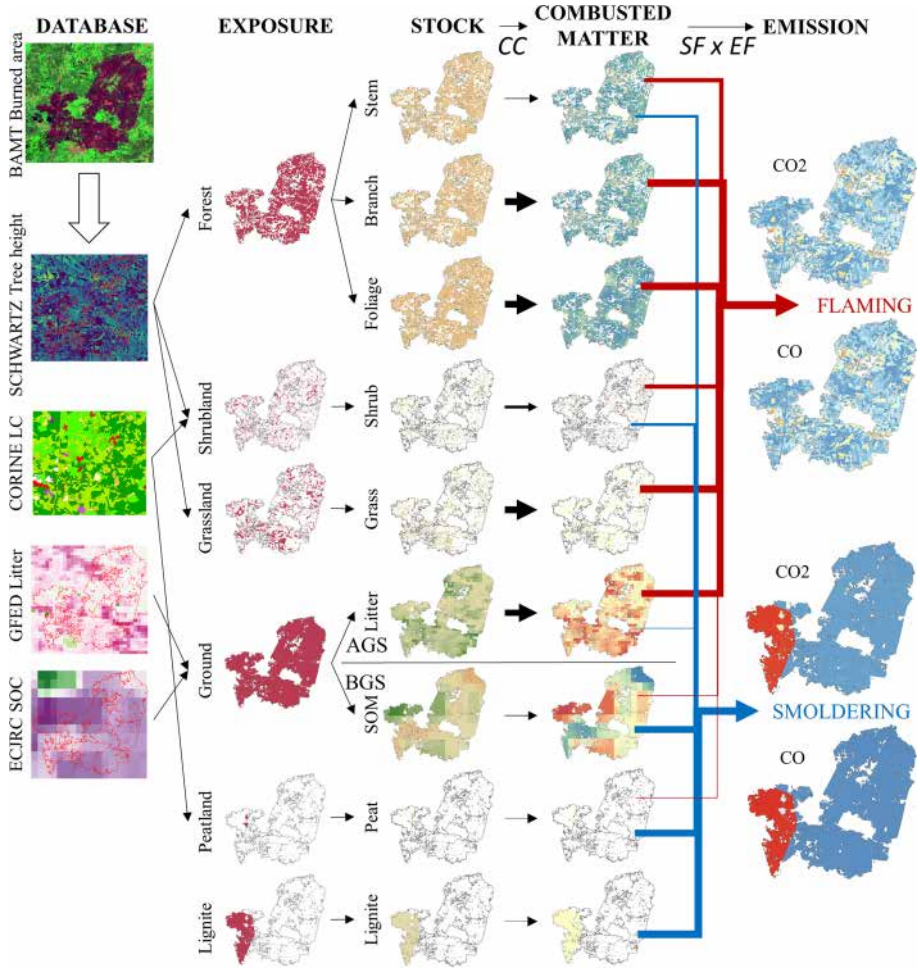

Figure 2. Refined fire emission model for temperate forest. The processing chain takes initial datasets as input to obtain exposure (burned area affecting each pool) and pool estimation (total amount of dry matter located in the burned area). Through specific values of combustion completeness (CC), smoldering fraction (SF), and emission factor (EF), the model calculates combusted matter (fraction of pool actually combusted) and emissions to the atmosphere (CO and CO_2) in the flaming and smoldering phases (see Table 2).

matter, fire emissions, and injection height on a daily basis since 2003, with near-real-time updates. We accessed GFAS data for CO_2 and CO emissions for the period spanning June to September 2022, considering the entire dataset within this time frame for our analysis.

3 Results

3.1 Attribution of the MCE to the various fires

In order to disentangle the inherent CO and CO_2 background mixing ratios at the atmospheric tower stemming from prevailing atmospheric conditions, and the emissions originating from actual fires, we initiated a rigorous assessment of our HYSPLIT atmospheric transport simulations and their alignment with the detected tower overpasses. Fire plume shapes and directions can be qualitatively evaluated when smoke is visible in visible satellite imagery. Figure 3 visually demonstrates the correspondence between observed plume positions, detected by MODIS, and the modeled plume positions, particularly in the case of the Landes fires. Notably, both the observed and modeled plumes exhibited a correct overlap, reinforcing the precision of our modeled wind direction changes as corroborated by the analysis of the comprehensive suite of satellite snapshots available throughout the study period.

It is worth mentioning that, during the same study period, TROPOMI data showed the arrival of an air mass with elevated CO concentrations from Spain, where forest fires were occurring at the same time (not shown here). However, we did not account for those fires in the current study, since the analysis of the HYSPLIT Lagrangian model results indicated a minimal impact from these fires on the time series monitored at the French towers, as evidenced by both forward- and backward-in-time simulations. Specifically, the results of the Lagrangian model indicated that the stations CRA and

Table 2. Synthesis table of parameters used in the refined fire emission model. Minimum and maximum combustion completeness (CC), smoldering fraction (SF) and emission factor (EF) for the smoldering (S) and flaming (F) combustions to CO and CO_2 are based on previously reported values in the carbon emission scientific literature. Intrinsic MCE values (MCEi) calculated from Eq. (2) are also provided.

Stock and pools	CC		SF	EF (g of gas per kg of DM pool)				MCEi	References
	Min	Max		CO_2		CO			
				F	S	F	S		
Aboveground stock (AGS)									
Stem	0.10	0.50	0.40	1700	1400	73	165	0.935	Van Wees et al. (2022), Prichard et al. (2020), Balde et al. (2023), Akagi et al. (2011)
Branch	0.90	1.00	0.00	1686		63		0.964	Van Wees et al. (2022), Prichard et al. (2020)
Leaf	0.90	1.00	0.00	1686		63		0.964	Van Wees et al. (2022), Prichard et al. (2020)
Shrub	0.40	0.99	0.40	1746	1460	72	93	0.953	Van Wees et al. (2022), Prichard et al. (2020), Akagi et al. (2011), Garcia-Hurtado et al. (2013)
Grass	0.90	1.00	0.00	1686		63		0.964	Van Wees et al. (2022), Prichard et al. (2020)
Litter	0.80	1.00	0.10	1696	1750	64	119	0.961	Van Wees et al. (2022), Prichard et al. (2020)
Belowground stock (BGS)									
SOM	0.10	0.50	0.90	1696	1000	64	298	0.796	Van Wees et al. (2022), Prichard et al. (2020)
Peat	0.05	0.20	0.90	1696	1000	64	298	0.796	Van Wees et al. (2022), Prichard et al. (2020), Akagi et al. (2011), Rein et al. (2009), Geron and Hays (2013)
Lignite	0.01	0.025	1.00		1500		750	0.666	Song et al. (2020)

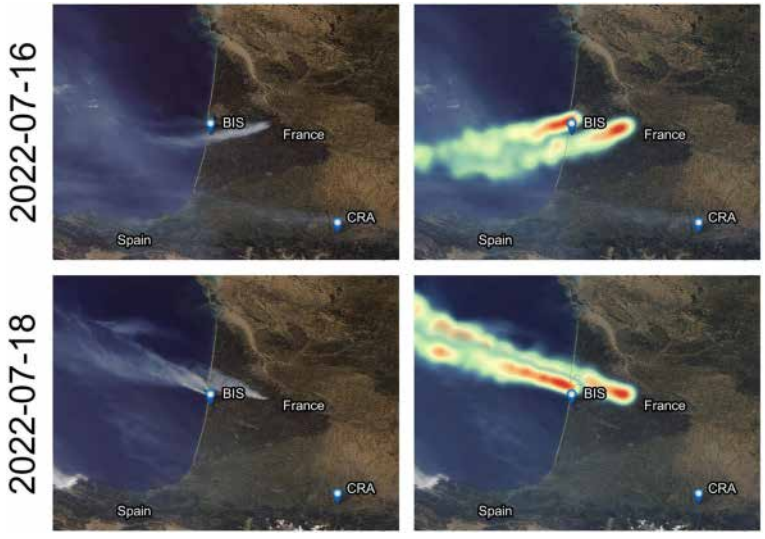

Figure 3. Overlay of the MODIS (observed, left column) and HYSPLIT (modeled, right column) plumes on 16 and 18 July 2022 during the Landes wildfires (red for the highest particle density, yellow for the lowest particle density).

PUY were largely unaffected by these fires. The analysis also showed that many signals from OHP were mixed with anthropogenic sources and had to be discarded. The plumes from both the Landiras and Monts d'Arrée fires were mixed before reaching the inland stations of MDH, OPE, SAC, and TRN. Consequently, we opted to exclude these towers from the MCE analysis, reserving their data solely for the evaluation of the RF background estimates. At each of the three remaining sites, namely BIS, OHP, and ROC, only the influence of the adjacent fire was observed: Landiras 1 for BIS, Montagnette for OHP, and Monts d'Arrée for ROC.

The analysis of the MCE index during the days when the simulated particles reached the atmospheric tower locations shows that the MCE signatures associated with the fires exhibit regional variations. In particular, the fire near BIS displayed a median MCE of 0.83 ± 0.03, the lowest mean value among the three sites (Fig. 4). The BIS values correspond to the MCE values that are observed most often under smoldering combustion phases and high-temperature pyrolysis phases. In contrast, the OHP fire predominantly featured MCEs exceeding 0.95, marked by low variations, with a minimum value of 0.93, primarily observed during flaming combustion. The ROC site collected intermediate values, with a median MCE of 0.94, close to the Mediterranean MCE observed at OHP. However, ROC exhibited minimum values that reached 0.82, far lower than the values observed at OHP. This variation suggests the occurrence of smoldering combustion phases throughout the fire propagation. Daily MCE variations (Fig. 4) emphasized a decreasing trend for the BIS fire, indicating an increase in smoldering combustion over time, supporting the hypothesis of a prolonged soil combustion following the cessation of the spreading stage. Conversely, this temporal pattern was less discernible for the fast-spreading ROC fire.

Furthermore, we looked into the 1 min averaged concentrations to investigate rapid changes in combustion, fire propagation, and atmospheric transport and the implications of different averaging periods on our analytical results. We found that the MCE values derived from both the 1 min and 1 h averaged mixing ratios are consistent, as shown in Fig. 4. While there is a broader dispersion in the case of the 1 min sampled mixing ratios, the fire MCE signal remained consistent across all stations. Notably, when accounting for the uncertainty in the RF estimates, the MCE varied by 2 % when propagating the mean error from the RF model for CO and CO_2. This variation had no discernible impact on the overall findings of this study, ensuring the consistent differentiation of the combustion types attributed to the main fires.

3.2 Exposure and stock affected

To disentangle the fire behaviors associated with the observed MCE indices measured at the towers located within the Atlantic temperate forest (ROC), Atlantic pine forest (BIS), and Mediterranean forest (OHP), we performed a comprehensive characterization of the affected AGS and BGS by these main fires.

Table 3. Description of the ROC, BIS, and OHP fires in terms of exposure (ha of vegetation and soil types affected), pool dry matter density ($t\,DM\,ha^{-1}$) for aboveground (stem, branch, leaf, shrub, grass, and litter) and belowground (SOM, peat, and lignite) pools, and the resulting total pool dry mass actually affected by the fires (t DM).

	ROC	BIS	OHP
Ignition date	18 July 2022	12 July 2022	14 July 2022
Duration	2 d	10 d	2 d
Exposure (ha)			
Fire	1726	12 140	1477
Forest	129	8622	1124
Shrubland	54	1257	226
Grassland	1093	2200	127
Soil	1276	12 078	1477
Peatland	449	61	
Lignite		1909	
Pool density ($t\,DM\,ha^{-1}$)			
Stem	25.0	40.7	42.3
Branch	8.5	13.8	14.4
Leaf	12.9	5.7	3.7
Shrub	7.8	7.3	10.0
Grass	4	4	4
Litter	5.0	7.3	3.8
SOM	140.1	235.7	95.2
Peat	2900.0	2900.0	
Lignite		14 000	
Pool dry mass (t DM)			
Stem	3.22×10^3	3.51×10^5	4.75×10^4
Branch	1.10×10^3	1.19×10^5	1.62×10^4
Leaf	2.36×10^3	5.61×10^4	4.97×10^3
Shrub	4.23×10^2	9.16×10^3	2.26×10^3
Grass	4.43×10^3	8.84×10^3	5.21×10^2
Litter	6.34×10^3	8.79×10^4	5.64×10^3
SOM	1.79×10^5	2.85×10^6	1.41×10^5
Peat	1.30×10^6	1.77×10^5	
Lignite		2.67×10^7	

The ROC fire, encompassing a total area of 1726 hectares, primarily impacted low vegetation, with grassland covering 63.3 % of the burned area (Table 3 and Fig. A2). The fire's influence on forest area was comparatively limited, spanning only 129 ha, characterized by a low biomass density of approximately $46\,t\,DM\,ha^{-1}$. A distinguishing feature of this fire is the substantial presence of peatland, occupying 449 ha (26 % of the burned area). Remarkably, the aggregated stock, combining AGS and BGS, is largely dominated by the peatland pool, accounting for 86.9 % of the total stock. We note here that this pool is recognized for its propensity to combust predominantly through smoldering.

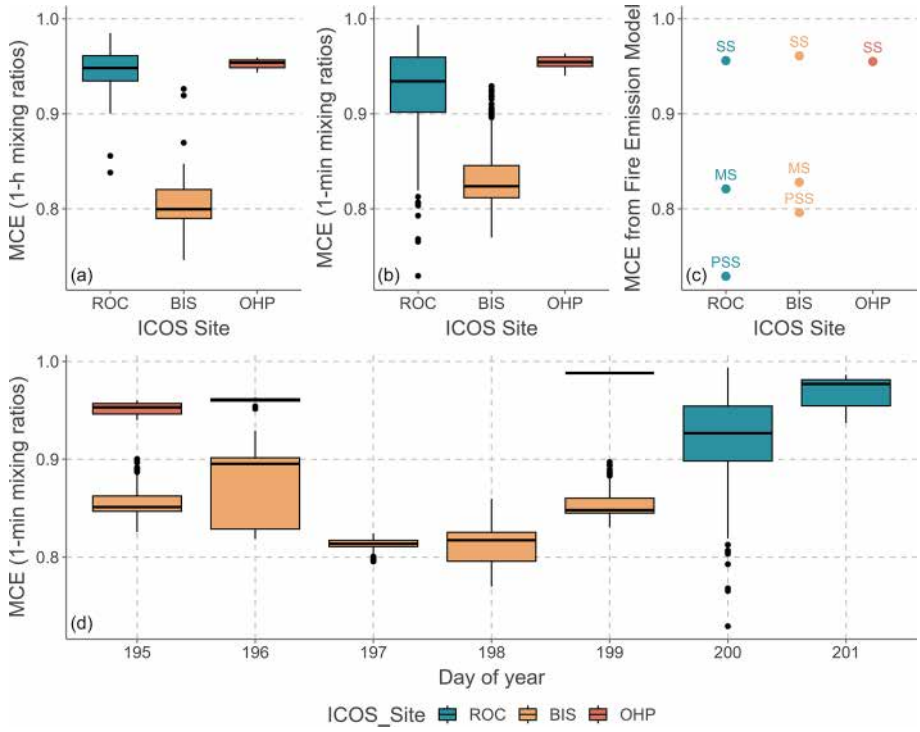

Figure 4. (a–c) Median and quartiles of the modified combustion efficiency (MCE) observed at the three atmospheric stations (ROC, BIS, and OHP) impacted by the nearby fires Monts d'Arrée, Landiras 1, and Montagnette, respectively. The left graph shows 1 h mixing ratios. The middle graph shows 1 min mixing ratios. The right graph shows the MCE obtained from the fire emission model (see Table 4). **(d)** Daily median and quartile values of the same corresponding data for 1 min mixing ratios.

The BIS fires extended over a considerably larger area of 12 140 ha and predominantly affected forested areas (71 % of the burned area) characterized by high biomass density ranging from 20 $t DM ha^{-1}$ to 150 $t DM ha^{-1}$ (see Fig. A2, "Vegetation"). Moreover, the SOM in this region falls within the highest range in the country, varying between 210 and 250 $t DM ha^{-1}$, a noticeably larger amount compared to the temperate Atlantic (100–220 $t DM ha^{-1}$) and Mediterranean (70–120 $t DM ha^{-1}$) regions (Fig. A2, "SOM"). Additionally, this fire also altered 61 hectares of peatland. An unusual feature of this area is the presence of a lignite layer situated near the surface, spanning 1909 hectares within the burned area (15.7 %). Remarkably, the lignite pool constitutes 88.0 % of the total dry matter stock (AGS and BGS), followed by the SOM pool (9.4 %). These two significant pools, lignite (combusted at high temperature during the pyrolysis phase) and SOM (mostly smoldering), both contribute to a substantial stock of carbon that is potentially affected, resulting in low MCEs.

Finally, the OHP fire in the Mediterranean region primarily affected forests (76.1 %), along with low vegetation zones like garrigue (consisting of 15.3 % shrubland and 8.6 % grassland). Forest biomass in this area, however, falls within the low range of biomass density observed in the country, with a median of 60.4 $t DM ha^{-1}$, and the soil contains relatively low amounts of organic matter (95.2 $t DM ha^{-1}$). Conversely, the aggregated stock (BGS and AGS) density, amounting to 147 $t DM ha^{-1}$, stands in stark contrast to the fires in Atlantic pine forests (2502 $t DM ha^{-1}$) or Atlantic temperate forests (867 $t DM ha^{-1}$).

As a first step toward identifying potential factors contributing to the lower MCEs in the BIS and ROC fires, we illustrate here that the fires with the lowest minimal MCEs (ROC and BIS) occurred in areas marked by the highest belowground organic density. Smoldering features shown by these fires have either been favored by carbon-enriched zones, such as peat bogs or lignite, or, as seen in the Landes region, featured a high SOM density.

3.3 Fire characterization

To discern whether specific fire characteristics could effectively distinguish fires affecting BGS, we conducted an assessment based on key parameters, such as the extent, duration, rate of spread, and intensity with 6-hourly fire radiative power (FRP).

Among the study sites, the maximum FRP was observed during the OHP fire, reaching 359 MW, followed by BIS with 299 MW and ROC with 150 MW (Fig. A3). ROC and OHP fires exhibited a relatively short duration of high FRP, extending up to 3 d, in contrast with the BIS fire, where the

period of high FRP persisted for 8 d. However, when examining low-intensity FRP, a discerning pattern emerged. The OHP fire showed no remaining burning activity beyond the initial 3 d of high-intensity combustion. In contrast, the ROC and BIS fires exhibited a protracted signal, spanning up to 25 d after ignition for ROC and 32 d after ignition for BIS (Fig. A3). This information appears pivotal for distinguishing fires characterized by low MCEs.

Furthermore, an evaluation of the fire rate of spread (ROS) within the burned area (Fig. 5) revealed distinct patterns. The BIS fire displayed a notably high hotspot density of $0.27\,\mathrm{hotspot\,ha^{-1}}$, combined with a relatively slow ROS at $0.147\,\mathrm{km\,h^{-1}}$. In contrast, the ROC fire expanded rapidly (median ROS of $1.77\,\mathrm{km\,h^{-1}}$), along with a markedly lower hotspot density of $0.055\,\mathrm{hotspot\,ha^{-1}}$. In particular, this fire spread relatively rapidly over grasslands, even when compared to the OHP fire, which occurred over shrublands and Mediterranean vegetation ($0.66\,\mathrm{km\,h^{-1}}$ with $0.05\,\mathrm{hotspots\,ha^{-1}}$).

Based on the characteristics related to propagation and combustion, we conclude that fires prone to experiencing smoldering combustion, such as BIS and ROC fires, exhibit a prolonged duration of hotspots after ignition, which is not observed for the OHP fire. This index could be used for a posteriori fire emission quantification but is hardly usable for near-real-time assessment. The median ROS and maximum fire intensity do not appear to be discriminating factors in fires impacting aboveground and belowground stocks.

3.4 Bottom-up approach to carbon emissions

Leveraging our estimation of both AGS and BGS in each of the BIS, ROC, and OHP fires, we undertook a bottom-up assessment of MCEs. This assessment compared our MCE estimates to the ranges of combustion and emission factor values estimated by previous studies. In our initial approach, we conducted the basic calculations akin to those employed in global fire emission models for temperate forests, exemplified by GFAS and FINN. This approach exclusively accounted for AGS and focused only on flaming combustion (Table 4, "AGS only"). The resulting MCEs ranged from 0.955 to 0.961 for all the fires, with no significant distinctions between them. While these values closely mirrored the median MCEs observed at the OHP tower with low variability, they notably diverged from the range of MCEs captured at the ROC and BIS stations.

In our subsequent approach, we incorporated belowground combustion effects for ROC and BIS. We divided the combustion process into three distinct stages (spreading stage, mixed stage, and post-spreading stage). For the ROC fire, the calculated MCE values for the spreading stage were 0.961 ($\pm$0.001), aligning with the median value obtained from the hourly mixing ratios measured at the ROC tower. Subsequently, for the mixed stage, MCE values of 0.828 ($\pm$0.015) were derived, corresponding to the lower range of 1 h mixing ratios. Finally, for the post-spreading stage, MCE values of 0.796 ($\pm$0.001) were obtained, similar to the minimum values observed within the distribution of the 1 min mixing ratio.

Considering the BIS fire, the results for the spreading stage exhibited MCE values of 0.956 ($\pm$0.004), values corresponding to the upper bounds of observations collected at the BIS tower. Subsequently, for the mixed stage, MCE values of 0.821 ($\pm$0.015) were calculated, representing the respective median values from the 1 h mixing ratio and the 1 min MCE. Finally, for the post-spreading stage, an MCE of 0.729 ($\pm$0.011) was derived, indicating a significant occurrence of smoldering combustion rate and closely mirroring the minimal values obtained for the 1 h MCE measured at this tower.

This refined bottom-up approach, including soil smoldering combustion, successfully captured the spectrum of MCEs observed at the ICOS atmospheric towers. These findings, which could not be obtained from aboveground combustion alone, underscore the significance of accounting for belowground combustion when addressing the carbon emission budget.

3.5 Fire emission assessment in 2022 for France

Drawing from our MCE-calibrated carbon emission framework of AGS and BGS combustion, we applied our refined carbon emission framework to the 70 fires exceeding 30 ha, which were accurately mapped across France. Smoldering combustion was exclusively attributed to fires affecting vegetation types similar to the BIS and ROC fires, namely those encompassing at least one of the following criteria: needle leaves and high SOM values, prolonged hotspot signal after the end of fire spread, and peatlands and/or lignite (Fig. A1).

The year 2022 witnessed a significant impact of fires in the Atlantic pine forest region, with a total burned area of 26 850 ha (Fig. 6), constituting 64.5 % of the overall burned area. Ranked second, the Mediterranean region experienced several fires over 7600 ha, accounting for 18.2 % of the total burned area. Fires mainly altered forest areas in the Atlantic pine region (76.5 %) and other forest regions (75.6 %). Regarding the Mediterranean region, fires influenced both forest (45.4 %) and low vegetation, including shrubland (11.0 %) and grassland (43.6 %). In the Atlantic temperate forest, grasslands were the most affected, encompassing 59.2 % of the burned area.

In our estimation, out of the total 44.68 Mt DM of stock impacted by fires in 2022 and potentially lost, only 4.526 ($\pm$2.138) MtDM was actually combusted and directly released into the atmosphere (Table A1). The Atlantic pine forest region contributed to the majority of this combusted matter due to its particularly large burned area and its substantial densities of AGS and BGS. More precisely, its AGS accounts for 28.2 % ($\pm$1.9) and its BGS for 54.1 % ($\pm$2.6). Moreover, the Atlantic temperate forest contributed significantly to the total stock combusted, when considering BGS,

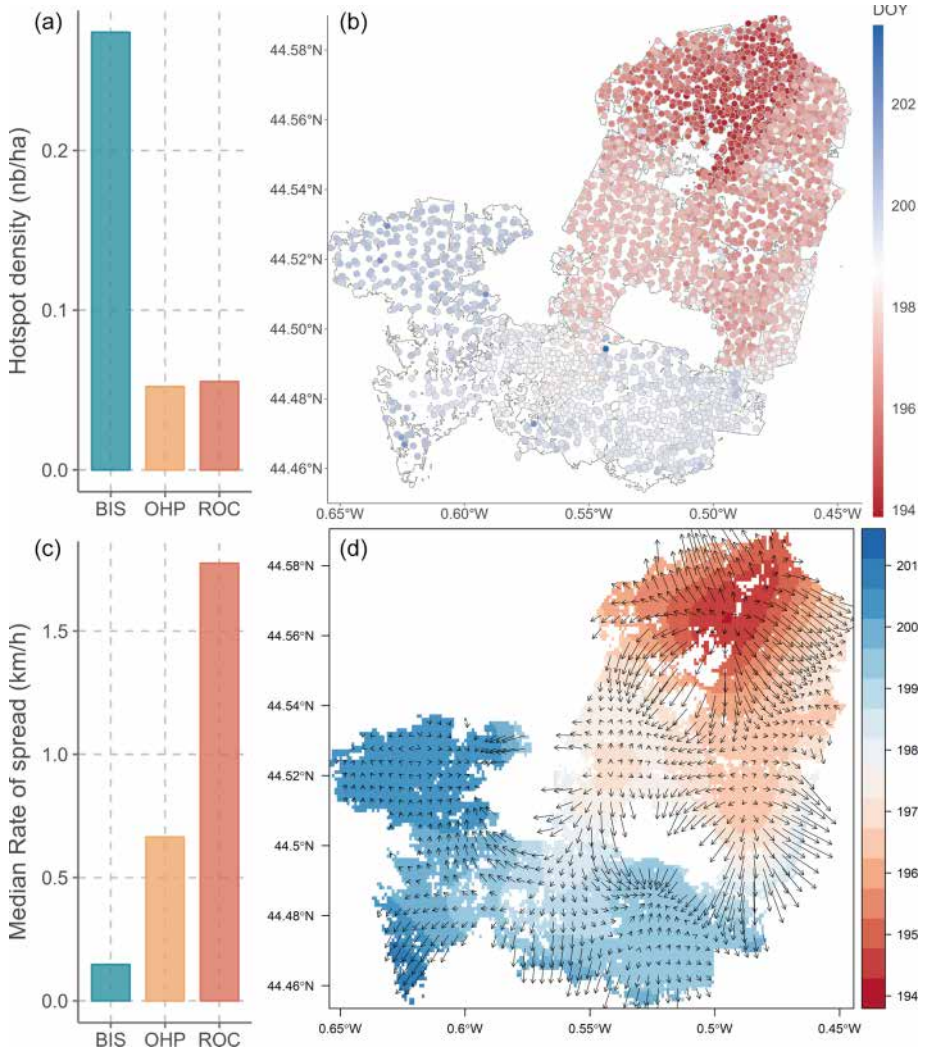

Figure 5. (a, b) Hotspot density ($nb\,ha^{-1}$) for each main fire and its corresponding flux tower (BIS, OHP, and ROC) and an example of hotspot distribution during the BIS fire (Landiras 1), with the corresponding day of year (DOY). **(c, d)** Median fire spread ($km\,h^{-1}$) for each main fire and its corresponding flux tower (BIS, OHP, and ROC) and an example of interpolated fire spread during the BIS fire. The color scale indicates the day of year of burning (decimal DOY), and arrows indicate the direction and rate of spread (proportional length of the arrow). Ignition corresponds to the pixel with the earliest DOY. We observed the change in spread direction, where the spread moved toward the southwest at first and then moved west and northwest, in accordance with changes in wind direction occurring during this fire (see Fig. 3).

primarily due to the presence of peatlands, accounting for 5.2 % ±0.3. In contrast, AGS combustion in the other three regions outside the Atlantic pine forest was responsible for only 12.5 % (±0.9) of the total stock loss.

Our estimates indicate that the fires of 2022 directly emitted 6.154 (±2.650) Mt of CO_2, with AGS and BGS contributing nearly equally to these CO_2 emissions. Specifically, all AGS was found to be responsible for 49.5 (±2.9) % of the annual CO_2 emissions, with the remainder attributed to BGS, particularly SOM and lignite from the Atlantic pine forest region (46.4 ± 2.7 %). In comparison, the GFAS framework estimated that summer fires were responsible for 3.86 Mt CO_2 emissions, when not considering mid-latitude extra-tropical potential BGS combustion and small peatland distribution, a value that corresponds to the lower bound of our estimations when considering our uncertainties on CC.

Taking into account soil combustion, we reach a value of 1.147 (±0.615) Mt CO emitted into the atmosphere. BGS combustion dominates the total CO emissions, representing 87.3 (±0.8) % of the annual emissions. We also note that the Atlantic pine forest region, through the combustion of its SOM and lignite, accounted for 81.6 (±0.6) % of the CO emissions. In stark contrast, GFAS provided markedly lower CO emissions with 0.204 Mt CO emitted during the 2022 fire season, which is 3 to 8 times lower than our estimates when excluding belowground combustion, depending on the mini-

Table 4. Bottom-up approach from stock to carbon emissions. Total pool dry matter combusted (tDM) and CO_2 and CO emission (in g) estimates are based on the parameters of Table 2. The resulting MCE is provided for each approach (considering only AGS or also including BGS), each fire, and each combustion stage. AGS: aboveground stock, BGS: belowground stock, SS: spreading stage, MS: mixed stage, PSS: post-spreading stage.

	Stock type	Matter combusted (t DM)	Emission (g)		MCE
			CO_2	CO	
AGS only					
ROC	AGS	1.45×10^4 ($\pm 1.80 \times 10^3$)	2.44×10^{10} ($\pm 2.97 \times 10^9$)	9.99×10^8 ($\pm 1.50 \times 10^8$)	0.961 ($\pm$0.001)
BIS	AGS	3.66×10^5 ($\pm 9.09 \times 10^4$)	6.06×10^{11} ($\pm 1.46 \times 10^{11}$)	2.86×10^{10} ($\pm 9.11 \times 10^9$)	0.956 ($\pm$0.004)
OHP	AGS	4.15×10^4 ($\pm 1.18 \times 10^4$)	6.84×10^{10} ($\pm 1.89 \times 10^{10}$)	3.34×10^9 ($\pm 1.20 \times 10^9$)	0.955 ($\pm$0.004)
AGS + BGS					
ROC					
SS					0.961 ($\pm$0.001)
	AGS	7.23×10^3 ($\pm 8.99 \times 10^2$)	1.22×10^{10} ($\pm 1.48 \times 10^9$)	4.99×10^8 ($\pm 7.49 \times 10^7$)	
MS					0.828 ($\pm$0.015)
	AGS	7.23×10^3 ($\pm 8.99 \times 10^2$)	1.22×10^{10} ($\pm 1.48 \times 10^9$)	4.99×10^8 ($\pm 7.49 \times 10^7$)	
	BGS	5.41×10^4 ($\pm 3.34 \times 10^4$)	5.79×10^{10} ($\pm 3.57 \times 10^{10}$)	1.49×10^{10} ($\pm 9.16 \times 10^9$)	
PSS					0.796 ($\pm$0.001)
	BGS	1.62×10^5 ($\pm 1.00 \times 10^5$)	1.74×10^{11} ($\pm 1.07 \times 10^{11}$)	4.46×10^{10} ($\pm 2.75 \times 10^{10}$)	
BIS					
SS					0.956 ($\pm$0.004)
	AGS	1.83×10^5 ($\pm 4.54 \times 10^4$)	3.03×10^{11} ($\pm 7.29 \times 10^{10}$)	1.43×10^{10} ($\pm 4.56 \times 10^9$)	
MS					0.821 ($\pm$0.015)
	AGS	1.83×10^5 ($\pm 4.54 \times 10^4$)	3.03×10^{11} ($\pm 7.29 \times 10^{10}$)	1.43×10^{10} ($\pm 4.56 \times 10^9$)	
	BGS	3.36×10^5 ($\pm 1.96 \times 10^5$)	4.10×10^{11} ($\pm 2.31 \times 10^{11}$)	1.48×10^{11} ($\pm 7.76 \times 10^{10}$)	
PSS					0.729 ($\pm$0.011)
	BGS	1.01×10^6 ($\pm 5.87 \times 10^5$)	1.23×10^{12} ($\pm 6.93 \times 10^{11}$)	4.44×10^{11} ($\pm 2.33 \times 10^{11}$)	

mum and maximum values of CC and other emission parameters in Table 2.

4 Discussion

4.1 Remote-sensing fire characterization for carbon emissions: beyond burned area

Remote-sensing information has played a key role in advancing our understanding of fire characteristics and their effects. Various studies have employed remote-sensing data to examine various aspects, such as estimates of burned areas (Chuvieco et al., 2019), fire sizes derived from aggregating burned pixel (Andela et al., 2019; Artés et al., 2019; Laurent et al., 2018, 2019), fire-spreading patterns based on burn dates within fire patches (Benali et al., 2016; Chen et al., 2022; Cardíl et al., 2023), fire intensities determined by fire radiative power (Wooster et al., 2021), and fire severity assessment (Alonso-González and Fernández-García, 2021). While these advancements provide valuable insights to characterize key features of fires driving combustion and carbon emission processes, it is important to acknowledge their limitations. These include the difficulty in detecting small fires, which can lead to an underestimation of burned areas (see Mouillot et al., 2014, for review) and challenges in accurately assessing fire intensity (Freeborn et al., 2014). Additionally, uncertainties persist in detecting burned areas in the forest understory (Roy et al., 2006) and in soils, peatlands (Atwood et al., 2016), and croplands (Hall et al., 2021). Combining information from both soil and vegetation fire types (Fisher et al., 2020; Sirin and Medvedeva, 2022) also remains a complex task. Efforts are currently underway to address these limitations through the development of more refined methods. These improvements encompass obtaining finer-resolution data for burned area (Chuvieco et al., 2022), enhancing the detection of understory fires (East et al., 2023), and providing more frequent and higher-resolution FRP datasets, such as those from VIIRS or stationary FRP information (Mota and Wooster, 2018). The use of hyperspectral sensors is also anticipated to offer new opportunities for improved fuel mapping, fire severity assessment, and combustion analysis (Veraverbeke et al., 2018).

Based on current remote-sensing strengths and weaknesses in fire characterization, we employed the most de-

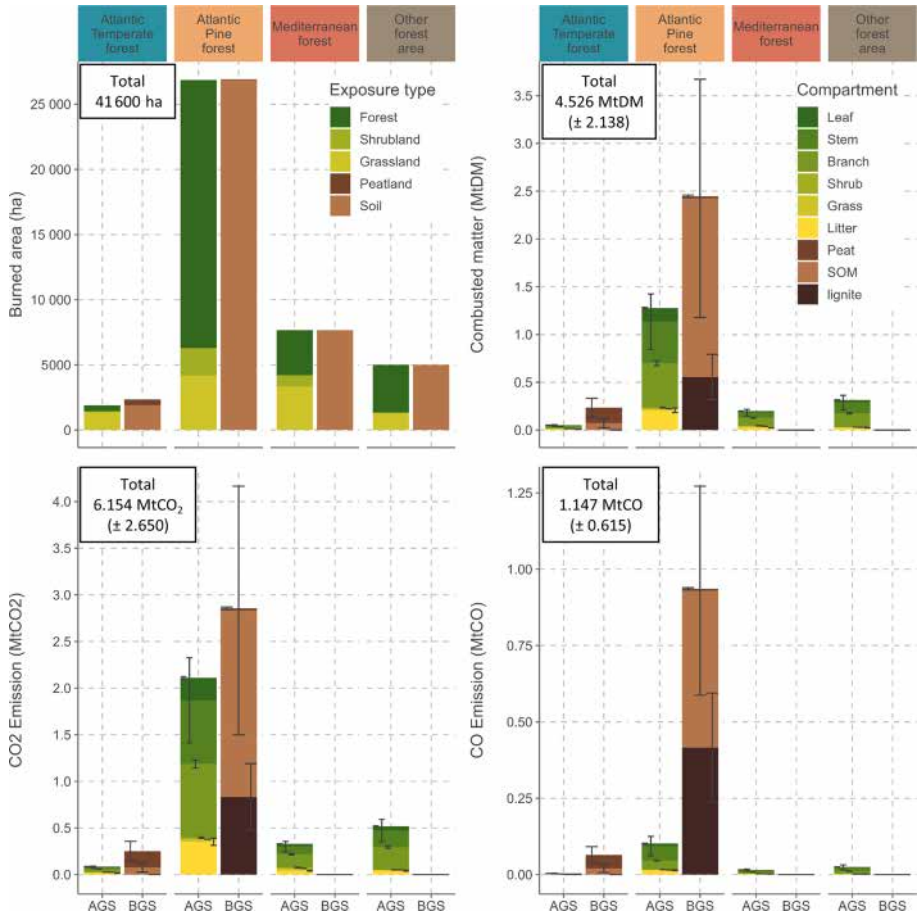

Figure 6. National footprint of France for the 2022 fire season. The burned area (ha), combusted matter (MtDM), CO_2, and CO (Mt) emissions are shown for each region, each stock type (AGS: aboveground stock, BGS: belowground stock), and each pool. Values are provided in Table A1.

tailed available data on burned areas and aboveground biomass in France. This fine-resolution dataset shows significant differences in burned estimates when compared to coarser-resolution information (Vallet et al., 2023b). We augmented this dataset with additional information on fire intensity, duration, and ROS, all of which were calculated from 6-hourly VIIRS FRP data, as has been done in previous studies in different regions (Benali et al., 2016; Chen et al., 2022; Cardíl et al., 2023).

An interesting addition to our analysis was the estimation of fire ROS, which exhibited considerable variability. ROS ranged from 1.7 $km\,h^{-1}$ in Brittany, predominantly affecting heathlands, to 0.7 $km\,h^{-1}$ in the Mediterranean Basin and even reached a significantly lower level in the Landes, not exceeding 0.2 $km\,h^{-1}$. Our estimates of fire spread fall within the range of previous ROS estimates, which varied between 0 and 30 $km\,d^{-1}$ (equivalent to 0–1.25 $km\,h^{-1}$) in California (Hantson et al., 2022), with notable impacts observed when ROS exceeds 0.8 $km\,d^{-1}$ and intensity surpasses 0.8 MW. For instance, Cardíl et al. (2023) estimated ROS values of 0.12, 0.17, and 0.19 $km\,h^{-1}$, respectively, for heathland, broadleaves, and pine forest based on hotspot data, while Salis et al. (2016) utilized fire-spread models to estimate ROS ranging from 0.12 to 3.6 $km\,h^{-1}$. However, higher ROS values have been observed in grasslands, ranging from 1.6 to 17 $km\,h^{-1}$ (Cruz et al., 2022). Mediterranean fires are known to be predominantly wind-driven in southern France (Ruffault and Mouillot, 2015), resulting in fast and unidirectional fire-spread patterns, which limits long fire residence time affecting soils. The northern region of France is windy on the Brittany coast and northern Channel shores, but wind speed remains lower across the southwest (Landes). Additionally, the Atlantic influence of fast-moving low-pressure systems going from west to east leads to daily changes in wind direction, as opposed to the long-lasting unidirectional mistral winds along the Mediterranean coast (Soukissian and Sotiriou, 2022). A noteworthy aspect related to intensity I (in MJ) is its relationship with heat release H, fuel consumption w, and rate of spread R (Alexander and Cruz, 2012). For a given intensity and heat release, fuel consumption is

inversely related to ROS due to increasing residence times. This relationship suggests that slower fires may be more prone to consuming larger fuel loads (Cobian-Iñiguez et al., 2022).

Regarding peatlands, previous studies have reported varying ROS values, with Cardíl et al. (2023) referring to $0.12\,km\,h^{-1}$ based on remotely sensed hotspots, while Huang and Rein (2017) only report $10\,cm\,h^{-1}$. This indicates that hotspots over peatland might represent the flaming of the surface, whereas the actual combustion of peat and fire progression occurs at a much slower pace and with lower intensity, making it challenging to fully capture by thermal anomalies.

In summary, our exploration of fire-spread processes in France has shown that the duration of hotspots within fire patches could serve as an effective and near-real-time indicator of soil combustion, which is closely related to smoldering combustion and, in turn, is shown by the low MCE values. This information on hotspot duration within fire patches has the potential to provide early warning signals for both populations and stakeholders, alerting them to potential air quality issues and the possibility of re-ignition (Xifré-Salvadó et al., 2020). Additionally, we recommend including this information as an additional key variable describing fire events in global fire patch databases (Laurent et al., 2018).

4.2 Pre-fire carbon stock uncertainties

In addition to assessing the extent of burned areas, the accuracy of carbon emission estimates is contingent upon the precision of the available biomass available for combustion. Recent enhancements in tree density and biomass estimation, encompassing isolated trees (Brandt et al., 2020) and more refined tree height data from lidar (Schwartz et al., 2023), have played a crucial role in improving the reliability of such estimates. These advancements, which we incorporated into our methodology, were discussed in Vallet et al. (2023a).

Estimates of SOM at regional and global levels (Lin et al., 2022; Vanguelova et al., 2016) have historically exhibited a relatively large level of uncertainty. We decided to rely on the ESDAC database (Yigini and Panagos, 2016), a strategy consistent with SOM observations available across the country (Martin et al., 2019). It is worth noting that deeper soil conditions better correspond to soil carbon information derived from biogeochemical models (Van Der Werf et al., 2017; Van Wees et al., 2022).

Exploring the effects of fires on the depth of soil burning has been a relatively understudied domain at a large scale. There is potential for improvement through lidar technology, which enables the identification of changes in soil surface thickness resulting from combustion (Reddy et al., 2015; Mickler et al., 2017), including low-severity peat fires (Bourgeau-Chavez et al., 2020). Peatlands, with their substantial stores of SOM, are susceptible to vertical spread rates, estimated at around $1\,cm\,h^{-1}$ by Huang and Rein (2017) or approximately $0.8\,cm\,h^{-1}$ ($0.–2.3\,cm\,h^{-1}$) in tropical peatlands (Graham et al., 2022). To maintain a conservative approach, we adopted a maximum ROS of $0.2\,cm\,h^{-1}$ for soil combustion, resulting in a daily consumption of approximately 4.8 cm, which roughly corresponds to 40 cm burned over an 8 d period, which corresponds to the average flaming duration of our fires. We computed peatland carbon stocks over a 2 m depth, with a combustion completeness (CC) varying between 0.05 and 0.2, thus affecting between 10 cm and the maximum value of 40 cm. This range of values of consumed peat aligns with conventional peatland emission models, often assuming 20 to 30 cm of peat being burned (Kohlenberg et al., 2018). However, it is worth noting that these parameters can vary from 1 cm to 54 cm in temperate peatlands in the UK (Davies et al., 2013). With this range of parameters, we reached an estimated carbon emission of 172 ($\pm$74) $t\,C\,ha^{-1}$ emitted (for a mean CC of 0.125 corresponding to 25 cm), which is higher than the value of $96\,t\,C\,ha^{-1}$ estimated by Davies et al. (2013) for US temperate forests. For a comparative perspective, Mickler et al. (2017), using fine-resolution lidar data, revealed that temperate peatland wildfires could exhibit an average burn depth of 42 cm, resulting in average belowground carbon emissions estimated at $544.43\,t\,C\,ha^{-1}$, highlighting the remaining uncertainty on the combustion of these carbon pools for temperate forest. In terms of peatlands cover referencing in France, the CORINE Land Cover database (EEA, 2019) was utilized to identify their exposure to fires. According to this source, the extent of wetland (marshland and peatland) in France stands at around 89 000 ha. However, we note here that this information remains highly uncertain, with different estimates varying between 275 000 and 300 000 ha, according to Tanneberger et al. (2017). This peatland extent would represent 0.52 % of the country, out of which 75 000 to 100 000 ha are regarded as mires. For another comparison point, Muller (2018) estimated the extent of French peatland at 59 000 ha, adding up uncertainty on the potential carbon emission from these fires under future climates and potential expansion of the pyroregions.

4.3 Atmospheric assessments of combustion

In addition to bottom-up approaches that rely on land surface combustion models and Earth observations, atmospheric fire emissions can also benefit from remote-sensing methods for detecting fire plumes and assessing their CO concentrations, as demonstrated by the TROPOMI sensor (Zhou et al., 2022). These remote-sensing data can be correlated with FRP (Griffin et al., 2024) and combustion efficiency (Van Der Velde et al., 2021). While it is important to validate these satellite data with actual atmospheric measurements, they offers valuable insights to study the impact of fire events (Yilmaz et al., 2023). Recent developments in this field (Vernooij et al., 2022) include the use of unoccupied aerial vehicles (UAVs), primarily applied to grasslands and savannas. This approach is particularly promising for assessing the seasonal variabil-

ity in emission factors (Vernooij et al., 2021). However, this measurement technique is restricted over forests, especially in Europe, where safety rules prevent the operation of aircraft or UAVs during firefighting interventions.

Our findings underscore that atmospheric tower measurements, while currently underutilized, represent an efficient and consistent surrogate, particularly for CO emissions (Wiggins et al., 2021). We have demonstrated the critical role of MCEs captured by the atmospheric mixing ratios in detecting smoldering combustion. Leveraging this information, we have enhanced the existing fire emission assessments for Europe under the Copernicus framework using the GFAS protocol (Kaiser et al., 2012). This enables our bottom-up approach to be confronted and evaluated against tower-measured MCEs, an independent approach to detecting and identifying fire behaviors.

The routine integration of these atmospheric data in future research holds the potential to unveil temporal patterns of flaming vs. smoldering combustion within fire events and across different seasons, in line with recent observations collected across various ecosystems (Carter et al., 2020; Zheng et al., 2018). Such an endeavor requires atmospheric inversion modeling due to the distance from the actual combustion source, with plume dynamics influenced by wind direction, which could introduce uncertainties related to meteorological data (Challa et al., 2008). Additionally, further investigations into emission factors for other greenhouse gases in the context of distinct fire types are warranted.

4.4 The 2022 fire-induced carbon emission budget

In our study, we took the year 2022 as a reference, a year marked by significant fire events in various ecosystems across France, which are representative of western Europe. A previous analysis conducted by Vallet et al. (2023a) already noted a substantial increase in biomass loss during 2022 in France, primarily due to an expanded burned area across the country. However, those conclusions were somewhat mitigated by the significant contribution of the low aboveground biomass affected by fires in Mediterranean shrublands and young managed forests in the Landes. It is worth noting that this previous study provided an estimate solely for potential aboveground biomass loss.

In our research, we extended the analysis to account for soil combustion, which we identified through MCE measurements from atmospheric towers. Consequently, our findings suggest that 7.95 ($\pm$3.63) $MtCO_2$-eq were emitted into the atmosphere during the 2022 fire season. Notably, 54.3 ($\pm$9.9) % of these emissions originated from the belowground biomass, with 35.4 ($\pm$10.4) % from peat and SOM and 18.95 ($\pm$0.65) % from lignite. These latter processes are often overlooked in fire emission assessment. In comparison, our estimates are 2-fold higher than the GFAS estimate of 4.18 $MtCO_2$-eq (CO and CO_2), which excludes these processes in temperate forest.

Consequently, fire represents a huge source of greenhouse gases. Considering that the national carbon footprint amounted to 403.8 $MtCO_2$-eq in 2022, fire represents 1.97 % ($\pm$0.89) of French emissions of greenhouse gases into the atmosphere (Citepa, 2023). Moreover, as forest is estimated to sequester 27 $MtCO_2$-eq per year in the country, fire disturbance would represent a reduction of 30 % in this carbon sink for this particular year.

One remarkable aspect of the 2022 fire season was the distinct impact on vegetation types (broadleaf vs. needle leaf), with varying rates of soil carbon accumulation. Temperate forests, characterized by a slower decomposition rate compared to the warmer Mediterranean climate, harbor more substantial litter and SOM density (Kurz-Besson et al., 2006). Additionally, our analysis revealed that the 2022 fires affected 510 ha of peatlands, as referenced in the CORINE Land Cover dataset, contributing to 2.6%–3.9 % of the total carbon emitted.

While carbon stock associated with charcoal or lignite is often ignored, located beneath the SOM layer, we demonstrated here that this contributor is significantly impacted during this unusual fire season. This particular combustion impacted 2265 ha over the lignite mines in the Landes, a phenomenon reported by local authorities and substantiated by our low MCE measurements. These low MCE values, which are challenging to account for based on biomass or SOM combustion alone, indicate the occurrence of lignite fires that could take place over an extended period. This phenomenon, reminiscent of the "zombie" fires recently observed, was reported by local authorities to have lasted even longer than expected over the winter 2022–2023 (McCarty et al., 2021; Irannezhad et al., 2020; Scholten et al., 2021; Kuklina et al., 2022). While lignite fires remain infrequent and are typically omitted in carbon emission inventories, they have been documented in other parts of the world (Stracher and Taylor, 2004; Brown, 2003; Fredriksson, 2002). These fires should raise concerns from authorities with additional preventive measures in France, especially in areas with superficial lignite deposits and accumulated carbon residues from historical charcoal basins, some of which have grown to a substantial height of 100 m in northern France (Anon, 2023).

Hotspot thermal anomalies and re-ignitions may persist up to 3 weeks after a fire, potentially emitting more carbon than our direct estimates suggest. These emissions, however, may be of a long-lasting nature but with a low intensity below the detection level of detection methods using atmospheric mixing ratios. Therefore, it is advisable to establish a more comprehensive measurement network to better understand and document this unexplored aspect of fire impact across European temperate forests.

Our results, while providing a preliminary and potentially conservative assessment of soil combustion in the region, underscore the need for enhanced field assessments of fire-induced effects on soil carbon stocks, particularly in peatlands and pine forests. These impacts could be even more

substantial than initially calculated, emphasizing the importance of further investigation.

4.5 Future directions for soil combustion modeling in Europe

Our investigation into fire emissions during the 2022 fire season in France carries significant insights that can be extended to applications across the entire European continent. Current global fire emission assessments, such as GFED, GFAS, and FINN, predominantly focus on the combustion of deep SOM in boreal regions and specific tropical peatlands. In contrast, regions like European temperate forests and, by extension, our study area are generally assumed to leave the soil unaffected by fire, except for litter burning (Van Wees et al., 2022).

One limitation in existing greenhouse gas emission inventories from fires is the failure to adequately account for the transition between the flaming and smoldering phases in aboveground biomass combustion. Following a study on fire emissions in California, Mebust et al. (2011) cautioned that current emission factors might overestimate the contribution of flaming combustion while underestimating the significance of smoldering combustion in total fire emissions. This concern was also raised in Europe by Garcia-Hurtado et al. (2013), who estimated that 25 % of emissions were associated with flaming and 75 % with smoldering. Our approach sought to address this limitation by considering these different combustion phases in our processing chain.

A second limitation in current carbon emission inventories pertains to the SOM accumulation and combustibility, which may have been previously underestimated. Recent studies have identified significant instances of smoldering combustion in areas where it was not previously considered, such as China's temperate forests (Tang et al., 2023) and even in African savannas towards the end of the burning season (Zheng et al., 2018). While temperate forests, characterized by milder temperatures and seasonal variations in soil moisture, were traditionally assumed to accumulate less carbon in soils compared to boreal forest, the actual situation is more nuanced. SOM levels (but also bulk density allowing oxygen transfer and better combustion) can vary locally in Europe, depending on factors like local climate and specific soil and leaf types. These traits, such as pH (Xiang et al., 2023) and leaf types (needles vs. broadleaves), can influence decomposition rates (Masuda et al., 2022; Krishna and Mohan, 2017; Cornelissen et al., 2011), highlighting the potential of using key plant traits as surrogates for SOM assessment. While SOM databases remain somewhat uncertain (Lin et al., 2022), insights from plant traits can be valuable.

The assumption that Mediterranean soils have been widely reported to hold low carbon stocks, thus not contributing to carbon emissions during fires, might not apply uniformly. For example, Certini et al. (2011) report that most carbon losses in Mediterranean pine forests (Tuscany, Italy) are attributable to the elimination of the litter layer rather than to changes in the underlying mineral soil carbon content, a conclusion also supported by Almendros and González-Vila (2012). This assumption might be true for broadleaf forests and shrublands, representing a large portion of burned area in Europe. However, smoldering combustion has been reported in some Mediterranean pine forests in Spain (Prat-Guitart et al., 2016), in central European Scotch pines, and in California for upper and lower duff (Garlough and Keyes, 2011), with moisture thresholds of 57 % and 102 % (Hille and Den Ouden, 2005). Our study confirmed smoldering combustion in temperate pine woodlands and heathlands. Therefore, we suggest that plant species distribution and their leaf traits, such as pH and leaf type, could be used to identify locations with substantial SOM accumulation, potentially leading to soil smoldering phases that should be included in carbon emission models. Notably, in higher latitudes (Turetsky et al., 2011b; Mekonnen et al., 2022; Walker et al., 2020) and eastern EU regions (Kirkland et al., 2023), carbon emissions from soil combustion can account for up to 90 % of the total carbon emitted. This has implications for the refinement of air quality estimates, which often rely on emissions derived from standard remote-sensing information and models (Menut et al., 2023).

We recommend the initiation and compilation of an emission factor inventory over Europe, following initiatives in the US and Canada (Prichard et al., 2020). Additionally, considering duff peat emissions and making more extensive use of the atmospheric tower network and fine-temporal-resolution remote sensing would enhance our understanding of fire events. Based on the boreal and tropical experience, peatland moisture content appears to be a critical factor influencing combustion depth and emission factors. Smoldering of biomass at lower moisture contents develops wider pyrolysis fronts that release a larger fraction of other gas species (Rein et al., 2009). Pyrolysis can even reach very low MCEs with large CO emissions (Song et al., 2020; Kohlenberg et al., 2018) when temperatures reach above 400 °C. Comprehensive models should integrate on-site peat and SOM moisture to account for changes in combustion rate and emission factors. This information has been available in France since 2016 through the peatland observation network (Bertrand et al., 2021; Gogo et al., 2021).

Understanding and predicting SOM and peat fire ignition and spread in temperate forests remains a relatively unexplored area of research due to the limited number of fire events as case studies. For instance, the ignition probability for SOM layers and peatlands is actually not yet fully understood. Pine cones have been identified as potentially influencing the ignition of soil duff (Kreye et al., 2013), thereby favoring smoldering, which is particularly relevant given that coniferous ecosystems tend to accumulate more SOM. Moreover, the spread of smoldering combustion is not well represented in current fire models, and its link with duff depth is minimal (Miyanishi and Johnson, 2002). The overall conse-

quences of soil smoldering combustion extend beyond carbon emissions, affecting ecological factors, such as the regeneration potential of seeder species like pines (Madrigal et al., 2010; Watts and Kobziar, 2013). Consequently, we echo the conclusion reached by Xifré-Salvadó et al. (2020) that SOM and peatland fires in France and in European temperate forests should be more deeply considered in terms of wildfire hazard, in particular for re-ignitions. For instance, the Landiras 1 fire exhibited smoldering combustion for 10 d before reigniting from its southwestern part over the lignite fires to ignite the Landiras 2 fire. Moreover, soil fires should be accounted for in forest planning and management, including soil fuel break strategies to halt smoldering combustion (Lin et al., 2021), in addition to the conventional focus on canopy fuel breaks.

5 Conclusion

This study offers compelling direct evidence of variable smoldering combustion rates observed during the atypical 2022 fire season. We employed the modified combustion efficiency ratio with atmospheric CO_2 and CO concentrations, calculated using data from the greenhouse gas atmospheric tower network situated throughout France. This particular year witnessed a significantly higher extent of burned area in the temperate Atlantic forest, marking a critical case study encompassing all major French sylvoecoregions. Our findings allow us to draw several important conclusions.

Firstly, we provided empirical support for the occurrence of soil, peatland, and even deeper lignite fires, phenomena that have previously been insufficiently demonstrated or evaluated through remotely sensed burn area data.

Secondly, we highlighted the large contribution of these fires within the overall carbon emission budget and trace gas emissions, which have not been fully integrated into existing fire emission models.

Lastly, our study enabled us to propose valuable warning signals for assessing re-ignition hazards and developing post-fire management strategies based on the duration and intensity of hotspots within the affected area and atmospheric tower data.

This research serves as a stepping stone for the development of future fire impact warning systems and emphasizes the potential of utilizing atmospheric greenhouse gas measurements in fire impact assessments. We also stress the need for enhanced vegetation and soil carbon emission factors during both flaming and smoldering phases. Finally, we advocate for efforts to update and further validate, from top-down approaches, the fire emission processing chain for European temperate forests.

Appendix A

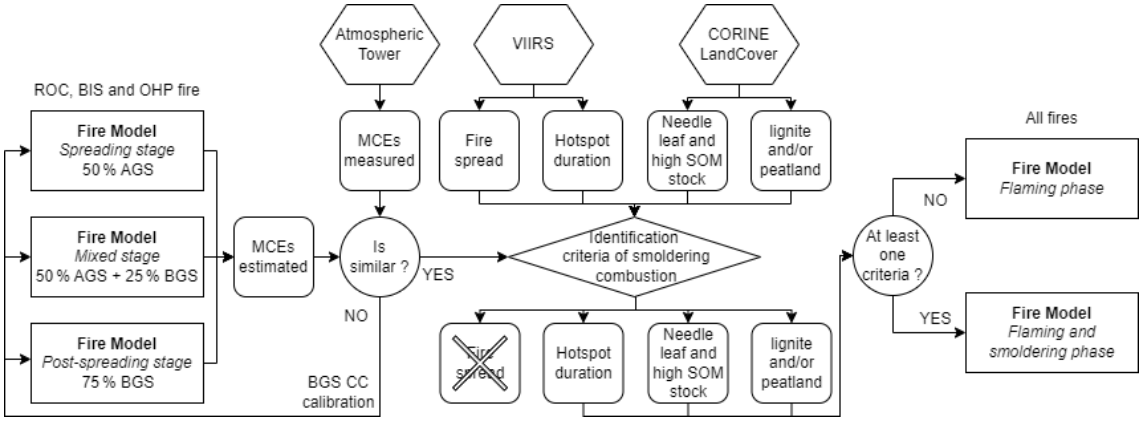

Figure A1. Fire model calibration process. AGS: aboveground Stock, BGS: belowground stock, MCE: modified combustion efficiency, SOM: soil organic matter.

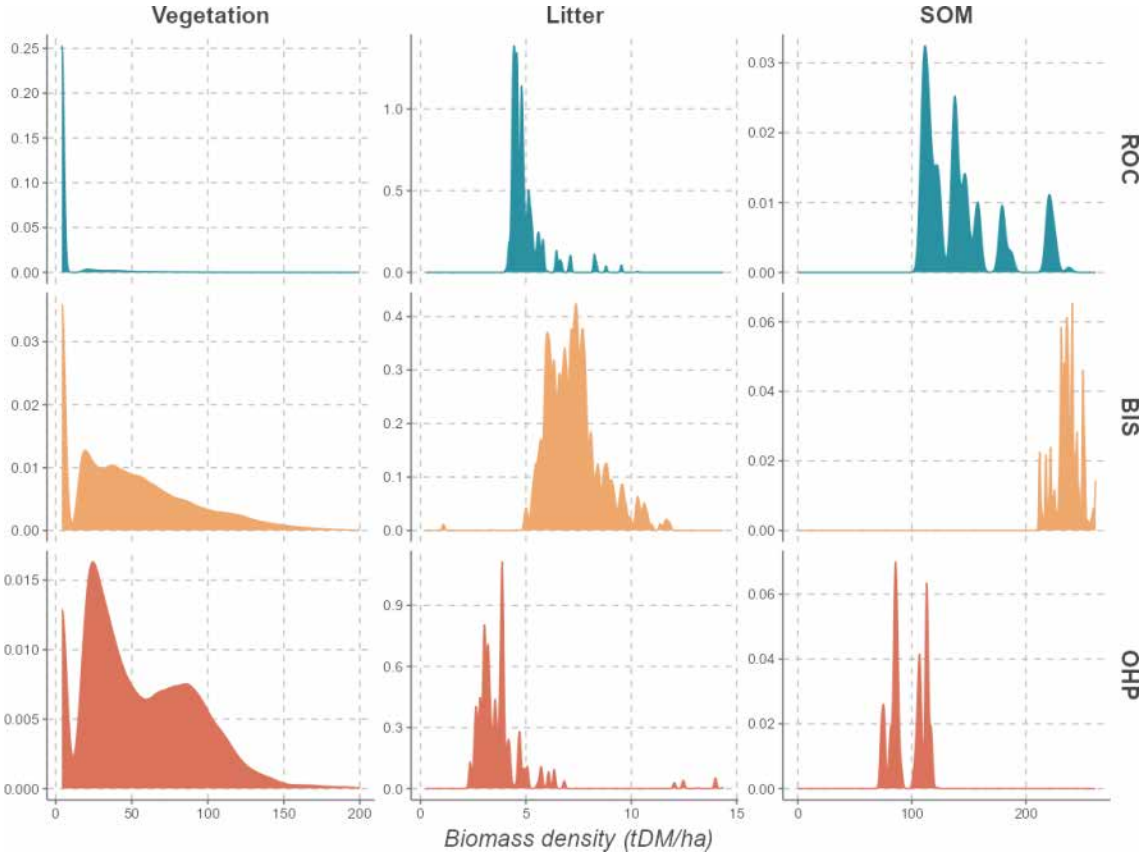

Figure A2. Vegetation biomass (stem, branch, leaf, shrub, and grass), litter, and SOM density ($\mathrm{tDM\,ha^{-1}}$) distribution for the BIS, ROC, and OHP fires.

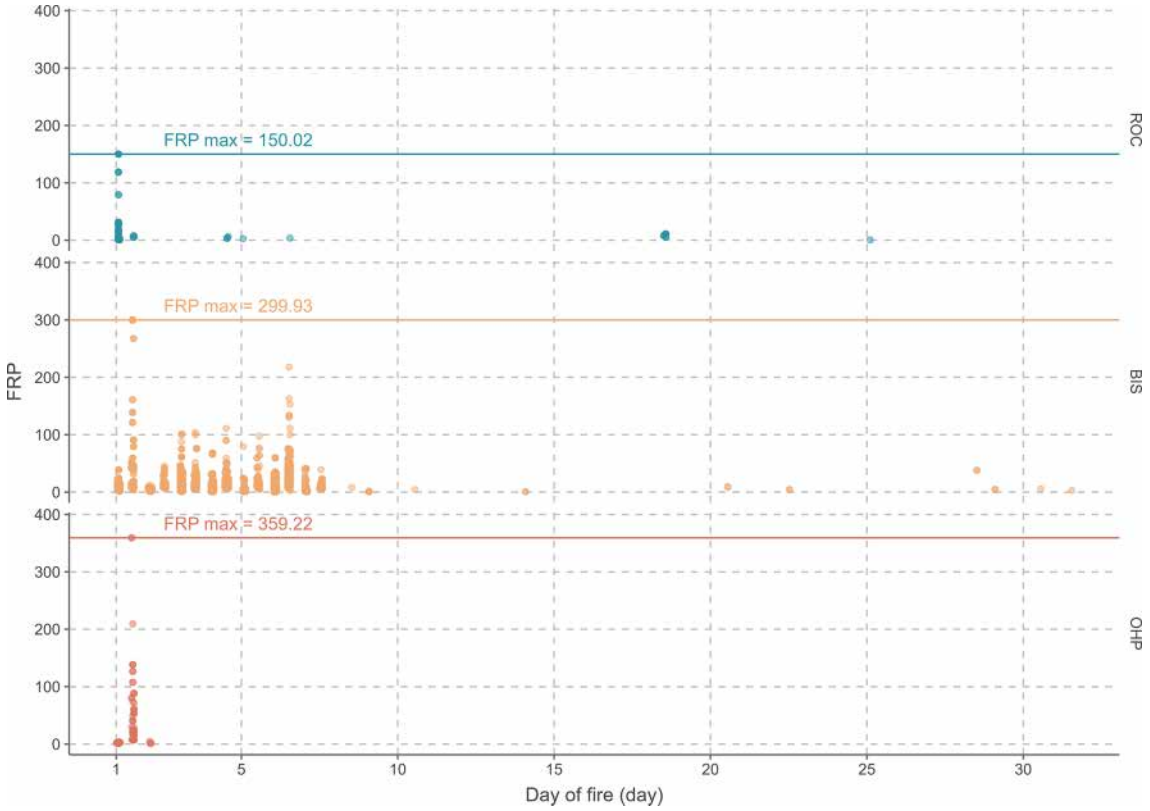

Figure A3. VIIRS/MCD14ML fire radiative power (FRP; in MW) temporal distribution from ignition to 5 weeks after ignition for each ROC, BIS, and OHP fire.

Table A1. Burned area (ha), stock (MtDM), matter combusted (MtDM), CO_2 and CO emissions (in Mt), resulting MCE, and GFAS estimation in France for the 2022 summer fire season and for the four regions.

Region	Burned area (ha)	Stock type	Stock (MtDM)	Matter combusted (MtDM)	Emission (Mt)		MCE	GFAS emission (Mt)	
					CO_2	CO		CO_2	CO
Atlantic temperate forest	2315	AGS BGS	0.081 1.546	0.052 (±0.010) 0.236 (±0.146)	0.086 (±0.017) 0.252 (±0.156)	0.004 (±0.001) 0.065 (±0.040)	0.841 (±0.017)	0.155	0.007
Atlantic pine forest	26 850	AGS BGS	2.351 38.121	1.278 (±0.350) 2.447 (±1.498)	2.111 (±0.559) 2.856 (±1.704)	0.102 (±0.036) 0.936 (±0.524)	0.834 (±0.015)	2.914	0.159
Mediterranean forest	7600	AGS BGS	0.332 0.850	0.199 (±0.046)	0.330 (±0.074)	0.015 (±0.005)	0.957 (±0.003)	0.272	0.014
Other forest area	4839	AGS BGS	0.590 0.808	0.315 (±0.087)	0.519 (±0.139)	0.025 (±0.009)	0.955 (±0.004)	0.516	0.024
Total	41 600		44.680	4.526 (±2.138)	6.154 (±2.650)	1.147 (±0.615)	7.172 (±0.081)	3.857	0.204

Data availability. Fire model emissions are available through the Easy data website: https://doi.org/10.57932/924f1b65-4032-40ce-879d-89a8348ee804 (Vallet and Mouillot, 2025).

Author contributions. LV, FM, and TL supervised the study framework. LV performed data curation and analysis on the fire emission model. LV, FM, and PC assembled the fire emission model and parameters. CA, LJ, and TL performed mixing ratio analysis. MR, ML, and IXR provided data from the atmospheric towers. LV, FM, and CA wrote the paper. All authors revised the paper.

Competing interests. The contact author has declared that none of the authors has any competing interests.

Disclaimer. Publisher's note: Copernicus Publications remains neutral with regard to jurisdictional claims made in the text, published maps, institutional affiliations, or any other geographical representation in this paper. While Copernicus Publications makes every effort to include appropriate place names, the final responsibility lies with the authors.

Acknowledgements. We would like to thank all of the partner projects listed in the financial support section for their contributions and the two reviewers for their fruitfull comments.

We thank the Service National d'Observation ICOS France Atmosphere (SIFA) for providing access to their atmospheric measurements data (https://www.aeris-data.fr/projects/icos-service-national-dobservation-icos-france-atmosphere-sifa/).

Financial support. This work was supported by the French Environment and Energy Management Agency (ADEME), the FirEUrisk H2020 project, the ANR FIRE-LANDES project (ANR-23-CE02-0031), the MSCA Staff Exchange FIRE-ADAPT project (no. 101086416), and the OSU OREME. The FirEUrisk project was granted funding from the European Union's Horizon 2020 research and innovation programme under grant agreement no. 101003890. This work was also supported by the Climate Change Initiative (CCI) Fire_cci project (contract no. 4000126706/19/INB).

Review statement. This paper was edited by Kirsten Thonicke and reviewed by Matthew Kasoar and one anonymous referee.

References

Akagi, S. K., Yokelson, R. J., Wiedinmyer, C., Alvarado, M. J., Reid, J. S., Karl, T., Crounse, J. D., and Wennberg, P. O.: Emission factors for open and domestic biomass burning for use in atmospheric models, Atmos. Chem. Phys., 11, 4039–4072, https://doi.org/10.5194/acp-11-4039-2011, 2011.

Alexander, M. E. and Cruz, M. G.: Modelling the effects of surface and crown fire behaviour on serotinous cone opening in jack pine and lodgepole pine forests, Int. J. Wildland Fire, 21, 709, https://doi.org/10.1071/WF11153, 2012.

Almendros, G. and González-Vila, F. J.: Wildfires, soil carbon balance and resilient organic matter in Mediterranean ecosystems. A review, Span. J. Soil Sci., 2, 153, https://doi.org/10.3232/SJSS.2012.V2.N2.01, 2012.

Alonso-González, E. and Fernández-García, V.: MOSEV: a global burn severity database from MODIS (2000–2020), Earth Syst. Sci. Data, 13, 1925–1938, https://doi.org/10.5194/essd-13-1925-2021, 2021.

Andela, N., Morton, D. C., Giglio, L., Paugam, R., Chen, Y., Hantson, S., van der Werf, G. R., and Randerson, J. T.: The Global Fire Atlas of individual fire size, duration, speed and direction, Earth Syst. Sci. Data, 11, 529–552, https://doi.org/10.5194/essd-11-529-2019, 2019.

Apphim: Les gisements de charbon et lignite, https://apphim.fr/articles.php?lng=fr&pg=6343&mnuid=1136&tconfig=0, last access: 22 September 2023.

Artés, T., Oom, D., De Rigo, D., Durrant, T. H., Maianti, P., Libertà, G., and San-Miguel-Ayanz, J.: A global wildfire dataset for the analysis of fire regimes and fire behaviour, Sci. Data, 6, 296, https://doi.org/10.1038/s41597-019-0312-2, 2019.

Asbjornsen, H., Velázquez-Rosas, N., García-Soriano, R., and Gallardo-Hernández, C.: Deep ground fires cause massive above- and below-ground biomass losses in tropical montane cloud forests in Oaxaca, Mexico, J. Trop. Ecol., 21, 427–434, https://doi.org/10.1017/S0266467405002373, 2005.

Astiani, D., Curran, L., Burhanuddin, Taherzadeh, M., Mujiman, Hatta, M., Pamungkas, W., and Gusmayanti, E.: Fire-driven Biomass and Peat Carbon Losses and Post-Fire Soil CO_2 Emission in a West Kalimantan Peatland Forest, J. Trop. For. Sci., 30, 570–575, https://doi.org/10.26525/jtfs2018.30.4.570575, 2018.

Atwood, E. C., Englhart, S., Lorenz, E., Halle, W., Wiedemann, W., and Siegert, F.: Detection and Characterization of Low Temperature Peat Fires during the 2015 Fire Catastrophe in Indonesia Using a New High-Sensitivity Fire Monitoring Satellite Sensor (FireBird), PLOS ONE, 11, e0159410, https://doi.org/10.1371/journal.pone.0159410, 2016.

Balde, B., Vega-Garcia, C., Gelabert, P. J., Ameztegui, A., and Rodrigues, M.: The relationship between fire severity and burning efficiency for estimating wildfire emissions in Mediterranean forests, J. For. Res., 34, 1195–1206, https://doi.org/10.1007/s11676-023-01599-1, 2023.

Bastarrika, A., Alvarado, M., Artano, K., Martinez, M., Mesanza, A., Torre, L., Ramo, R., and Chuvieco, E.: BAMS: A Tool for Supervised Burned Area Mapping Using Landsat Data, Remote Sens., 6, 12360–12380, https://doi.org/10.3390/rs61212360, 2014.

Belgiu, M. and Drăguţ, L.: Random forest in remote sensing: A review of applications and future directions, ISPRS J. Photogramm., 114, 24–31, https://doi.org/10.1016/j.isprsjprs.2016.01.011, 2016.

Benali, A., Russo, A., Sá, A., Pinto, R., Price, O., Koutsias, N., and Pereira, J.: Determining Fire Dates and Locating Ignition Points With Satellite Data, Remote Sens., 8, 326, https://doi.org/10.3390/rs8040326, 2016.

Bertrand, G., Ponçot, A., Pohl, B., Lhosmot, A., Steinmann, M., Johannet, A., Pinel, S., Caldirak, H., Artigue, G., Binet, P., Bertrand, C., Collin, L., Magnon, G., Gilbert, D., Laggoun-Deffarge, F., and Toussaint, M.-L.: Statistical hydrology for evaluating peatland water table sensitivity to simple environmental variables and climate changes application to the mid-latitude/altitude Frasne peatland (Jura Mountains, France), Sci. Total Environ., 754, 141931, https://doi.org/10.1016/j.scitotenv.2020.141931, 2021.

Bourgeau-Chavez, L. L., Grelik, S. L., Billmire, M., Jenkins, L. K., Kasischke, E. S., and Turetsky, M. R.: Assessing Boreal Peat Fire Severity and Vulnerability of Peatlands to Early Season Wildland Fire, Frontiers in Forests and Global Change, 3, 20, https://doi.org/10.3389/ffgc.2020.00020, 2020.

Brandt, M., Tucker, C. J., Kariryaa, A., Rasmussen, K., Abel, C., Small, J., Chave, J., Rasmussen, L. V., Hiernaux, P., Diouf, A. A., Kergoat, L., Mertz, O., Igel, C., Gieseke, F., Schöning, J., Li, S., Melocik, K., Meyer, J., Sinno, S., Romero, E., Glennie, E., Montagu, A., Dendoncker, M., and Fensholt, R.: An unexpectedly large count of trees in the West African Sahara and Sahel, Nature, 587, 78–82, https://doi.org/10.1038/s41586-020-2824-5, 2020.

Breiman, L.: Random Forests, Mach. Learn., 45, 5–32, https://doi.org/10.1023/A:1010933404324, 2001.

Brown, K.: Subterranean Coal Fires Spark Disaster, Science, 299, 1177–1177, https://doi.org/10.1126/science.299.5610.1177b, 2003.

CAMS: Copernicus, https://atmosphere.copernicus.eu/global-fire-emissions, last access: 22 September 2023.

Cardíl, A., Tapia, V. M., Monedero, S., Quiñones, T., Little, K., Stoof, C. R., Ramirez, J., and de-Miguel, S.: Characterizing the rate of spread of large wildfires in emerging fire environments of northwestern Europe using Visible Infrared Imaging Radiometer Suite active fire data, Nat. Hazards Earth Syst. Sci., 23, 361–373, https://doi.org/10.5194/nhess-23-361-2023, 2023.

Carter, T. S., Heald, C. L., Jimenez, J. L., Campuzano-Jost, P., Kondo, Y., Moteki, N., Schwarz, J. P., Wiedinmyer, C., Darmenov, A. S., da Silva, A. M., and Kaiser, J. W.: How emissions uncertainty influences the distribution and radiative impacts of smoke from fires in North America, Atmos. Chem. Phys., 20, 2073–2097, https://doi.org/10.5194/acp-20-2073-2020, 2020.

Certini, G., Nocentini, C., Knicker, H., Arfaioli, P., and Rumpel, C.: Wildfire effects on soil organic matter quantity and quality in two fire-prone Mediterranean pine forests, Geoderma, 167–168, 148–155, https://doi.org/10.1016/j.geoderma.2011.09.005, 2011.

Challa, V. S., Indrcanti, J., Baham, J. M., Patrick, C., Rabarison, M. K., Young, J. H., Hughes, R., Swanier, S. J., Hardy, M. G., and Yerramilli, A.: Sensitivity of atmospheric dispersion simulations by HYSPLIT to the meteorological predictions from a meso-scale model, Environ. Fluid Mech., 8, 367–387, https://doi.org/10.1007/s10652-008-9098-z, 2008.

Chen, Y., Hantson, S., Andela, N., Coffield, S. R., Graff, C. A., Morton, D. C., Ott, L. E., Foufoula-Georgiou, E., Smyth, P., Goulden, M. L., and Randerson, J. T.: California wildfire spread derived using VIIRS satellite observations and an object-based tracking system, Sci. Data, 9, 249, https://doi.org/10.1038/s41597-022-01343-0, 2022.

Chuvieco, E., Mouillot, F., Van Der Werf, G. R., San Miguel, J., Tanase, M., Koutsias, N., García, M., Yebra, M., Padilla, M., Gitas, I., Heil, A., Hawbaker, T. J., and Giglio, L.: Historical background and current developments for mapping burned area from satellite Earth observation, Remote Sens. Environ., 225, 45–64, https://doi.org/10.1016/j.rse.2019.02.013, 2019.

Chuvieco, E., Roteta, E., Sali, M., Stroppiana, D., Boettcher, M., Kirches, G., Storm, T., Khairoun, A., Pettinari, M. L., Franquesa, M., and Albergel, C.: Building a small fire database for Sub-Saharan Africa from Sentinel-2 high-resolution images, Sci. Total Environ., 845, 157139, https://doi.org/10.1016/j.scitotenv.2022.157139, 2022.

Chuvieco, E., Yebra, M., Martino, S., Thonicke, K., Gómez-Giménez, M., San-Miguel, J., Oom, D., Velea, R., Mouillot, F., Molina, J. R., Miranda, A. I., Lopes, D., Salis, M., Bugaric, M., Sofiev, M., Kadantsev, E., Gitas, I. Z., Stavrakoudis, D., Eftychidis, G., Bar-Massada, A., Neidermeier, A., Pampanoni, V., Pettinari, M. L., Arrogante-Funes, F., Ochoa, C., Moreira, B., and Viegas, D.: Towards an Integrated Approach to Wildfire Risk Assessment: When, Where, What and How May the Landscapes Burn, Fire, 6, 215, https://doi.org/10.3390/fire6050215, 2023.

Citepa: Gaz à effet de serre et polluants atmosphériques, Bilan des émissions en France de 1990 à 2022, Rapport Secten, https://www.citepa.org/wp-content/uploads/publications/secten/2023/Citepa_Secten_ed2023_v1.pdf (last access: 8 January 2025), 2023.

Cobian-Iñiguez, J., Richter, F., Carmignani, L., Liveretou, C., Xiong, H., Stephens, S., Finney, M., Gollner, M., and Fernandez-Pello, C.: Wind Effects on Smoldering Behavior of Simulated Wildland Fuels, Combust. Sci. Technol., 1–18, https://doi.org/10.1080/00102202.2021.2019239, 2022.

Conil, S., Helle, J., Langrene, L., Laurent, O., Delmotte, M., and Ramonet, M.: Continuous atmospheric CO_2, CH_4 and CO measurements at the Observatoire Pérenne de l'Environnement (OPE) station in France from 2011 to 2018, Atmos. Meas. Tech., 12, 6361–6383, https://doi.org/10.5194/amt-12-6361-2019, 2019.

Cornelissen, J. H. C., Sibma, F., Van Logtestijn, R. S. P., Broekman, R. A., and Thompson, K.: Leaf pH as a plant trait: species-driven rather than soil-driven variation: Species versus soil chemistry effects on leaf pH, Funct. Ecol., 25, 449–455, https://doi.org/10.1111/j.1365-2435.2010.01765.x, 2011.

Cruz, M. G., Alexander, M. E., and Kilinc, M.: Wildfire Rates of Spread in Grasslands under Critical Burning Conditions, Fire, 5, 55, https://doi.org/10.3390/fire5020055, 2022.

Davies, G. M., Gray, A., Rein, G., and Legg, C. J.: Peat consumption and carbon loss due to smouldering wildfire in a temperate peatland, Forest Ecol. Manag., 308, 169–177, https://doi.org/10.1016/j.foreco.2013.07.051, 2013.

De Vos, B., Cools, N., Ilvesniemi, H., Vesterdal, L., Vanguelova, E., and Carnicelli, S.: Benchmark values for forest soil carbon stocks in Europe: Results from a large scale forest soil survey, Geoderma, 251–252, 33–46, https://doi.org/10.1016/j.geoderma.2015.03.008, 2015.

Desservettaz, M. J., Fisher, J. A., Luhar, A. K., Woodhouse, M. T., Bukosa, B., Buchholz, R. R., Wiedinmyer, C., Griffith, D. W. T., Krummel, P. B., Jones, N. B., Deutscher, N. M., and Greenslade, J. W.: Australian Fire Emissions of Carbon Monoxide Estimated by Global Biomass Burning Inventories: Variability and Observational Constraints, J. Geophys. Res.-Atmos., 127, e2021JD035925, https://doi.org/10.1029/2021JD035925, 2022.

East, A., Hansen, A., Armenteras, D., Jantz, P., and Roberts, D. W.: Measuring Understory Fire Effects from Space: Canopy Change in Response to Tropical Understory Fire and What This Means for Applications of GEDI to Tropical Forest Fire, Remote Sens., 15, 696, https://doi.org/10.3390/rs15030696, 2023.

EEA: CORINE Land Cover 2018, EEA, https://doi.org/10.2909/960998c1-1870-4e82-8051-6485205ebbac, https://land.copernicus.eu/pan-european/corine-land-cover/clc2018 (last access: 2 February 2023), 2019.

European Commission, Joint Research Centre: Advance report on forest fires in Europe, Middle East and North Africa 2022, Publications Office, LU, 2023.

Fernández-Guisuraga, J. M., Calvo, L., Fernandes, P. M., and Suárez-Seoane, S.: Short-Term Recovery of the Aboveground Carbon Stock in Iberian Shrublands at the Extremes of an Environmental Gradient and as a Function of Burn Severity, Forests, 13, 145, https://doi.org/10.3390/f13020145, 2022.

Fisher, D., Wooster, M. J., Xu, W., Thomas, G., and Lestari, P.: Top-Down Estimation of Particulate Matter Emissions from Extreme Tropical Peatland Fires Using Geostationary Satellite Fire Radiative Power Observations, Sensors, 20, 7075, https://doi.org/10.3390/s20247075, 2020.

Franquesa, M., Vanderhoof, M. K., Stavrakoudis, D., Gitas, I. Z., Roteta, E., Padilla, M., and Chuvieco, E.: Development of a standard database of reference sites for validating global burned area products, Earth Syst. Sci. Data, 12, 3229–3246, https://doi.org/10.5194/essd-12-3229-2020, 2020.

Fredriksson, G. M.: Extinguishing the 1998 forest fires and subsequent coal fires in the Sungai Wain Protection Forest, East Kalimantan, Indonesia, in: Communities in flames: proceedings of an international conference on community involvement in fire management, edited by: Moore, P., Ganz, D., Tan, L. C., Enters, T., and Durst, P. B., Bangkok, Thailand, FAO and FireFight SE Asia, 74–81, 2002.

Freeborn, P. H., Wooster, M. J., Roy, D. P., and Cochrane, M. A.: Quantification of MODIS fire radiative power (FRP) measurement uncertainty for use in satellite-based active fire characterization and biomass burning estimation, Geophys. Res. Lett., 41, 1988–1994, https://doi.org/10.1002/2013GL059086, 2014.

Galizia, L. F., Barbero, R., Rodrigues, M., Ruffault, J., Pimont, F., and Curt, T.: Global Warming Reshapes European Pyroregions, Earths Future, 11, e2022EF003182, https://doi.org/10.1029/2022EF003182, 2023.

García, M. J. L. and Caselles, V.: Mapping burns and natural reforestation using thematic Mapper data, Geocarto Int., 6, 31–37, https://doi.org/10.1080/10106049109354290, 1991.

Garcia-Hurtado, E., Pey, J., Baeza, M. J., Carrara, A., Llovet, J., Querol, X., Alastuey, A., and Vallejo, V. R.: Carbon emissions in Mediterranean shrubland wildfires: An experimental approach, Atmos. Environ., 69, 86–93, https://doi.org/10.1016/j.atmosenv.2012.11.063, 2013.

Garlough, E. C. and Keyes, C. R.: Influences of moisture content, mineral content and bulk density on smouldering combustion of ponderosa pine duff mounds, Int. J. Wildland Fire, 20, 589, https://doi.org/10.1071/WF10048, 2011.

Geron, C. and Hays, M.: Air emissions from organic soil burning on the coastal plain of North Carolina, Atmos. Environ., 64, 192–199, https://doi.org/10.1016/j.atmosenv.2012.09.065, 2013.

Gerrand, S., Aspinall, J., Jensen, T., Hopkinson, C., Collingwood, A., and Chasmer, L.: Partitioning carbon losses from fire combustion in a montane Valley, Alberta Canada, Forest Ecol. Manag., 496, 119435, https://doi.org/10.1016/j.foreco.2021.119435, 2021.

Giglio, L., Schroeder, W., and Justice, C. O.: The collection 6 MODIS active fire detection algorithm and fire products, Remote Sens. Environ., 178, 31–41, https://doi.org/10.1016/j.rse.2016.02.054, 2016.

Gogo, S., Paroissien, J., Laggoun-Défarge, F., Antoine, J., Bernard-Jannin, L., Bertrand, G., Binet, P., Binet, S., Bouger, G., Brossard, Y., Camboulive, T., Caudal, J., Chevrier, S., Chiapiuso, G., D'Angelo, B., Durantez, P., Flechard, C., Francez, A., Galop, D., Gandois, L., Gilbert, D., Guimbaud, C., Hinault, L., Jacotot, A., Le Moing, F., Lerigoleur, E., Le Roux, G., Leroy, F., Lhosmot, A., Li, Q., Machado Da Silva, E., Moquet, J., Mora-Gomez, J., Perdereau, L., Rosset, T., and Toussaint, M.: The information system of the French Peatland Observation Service: Service National d'Observation Tourbières – A valuable tool to assess the impact of global changes on the hydrology and biogeochemistry of temperate peatlands through long term monitoring, Hydrol. Process., 35, e14244, https://doi.org/10.1002/hyp.14244, 2021.

Graham, L. L. B., Applegate, G. B., Thomas, A., Ryan, K. C., Saharjo, B. H., and Cochrane, M. A.: A Field Study of Tropical Peat Fire Behaviour and Associated Carbon Emissions, Fire, 5, 62, https://doi.org/10.3390/fire5030062, 2022.

Gräler, B., Pebesma, E., and Heuvelink, G.: Spatio-Temporal Interpolation using gstat, R. J., 8, 204–218, 2016.

Griffin, D., Chen, J., Anderson, K., Makar, P., McLinden, C. A., Dammers, E., and Fogal, A.: Biomass burning CO emissions: exploring insights through TROPOMI-derived emissions and emission coefficients, Atmos. Chem. Phys., 24, 10159–10186, https://doi.org/10.5194/acp-24-10159-2024, 2024.

Hall, J. V., Zibtsev, S. V., Giglio, L., Skakun, S., Myroniuk, V., Zhuravel, O., Goldammer, J. G., and Kussul, N.: Environmental and political implications of underestimated cropland burning in Ukraine, Environ. Res. Lett., 16, 064019, https://doi.org/10.1088/1748-9326/abfc04, 2021.

Hantson, S., Andela, N., Goulden, M. L., and Randerson, J. T.: Human-ignited fires result in more extreme fire behavior and ecosystem impacts, Nat. Commun., 13, 2717, https://doi.org/10.1038/s41467-022-30030-2, 2022.

Hao, W. M. and Ward, D. E.: Methane production from global biomass burning, J. Geophys. Res.-Atmos., 98, 20657–20661, https://doi.org/10.1029/93JD01908, 1993.

Heiskanen, J., Brümmer, C., Buchmann, N., Calfapietra, C., Chen, H., Gielen, B., Gkritzalis, T., Hammer, S., Hartman, S., Herbst, M., Janssens, I. A., Jordan, A., Juurola, E., Karstens, U., Kasurinen, V., Kruijt, B., Lankreijer, H., Levin, I., Linderson, M.-L., Loustau, D., Merbold, L., Myhre, C. L., Papale, D., Pavelka, M., Pilegaard, K., Ramonet, M., Rebmann, C., Rinne, J., Rivier, L., Saltikoff, E., Sanders, R., Steinbacher, M., Steinhoff, T., Watson, A., Vermeulen, A. T., Vesala, T., Vítková, G., and Kutsch, W.: The Integrated Carbon Observation System in Europe, B. Am. Meteorol. Soc., 103, E855–E872, https://doi.org/10.1175/BAMS-D-19-0364.1, 2022.

Hersbach, H., Bell, B., Berrisford, P., Hirahara, S., Horányi, A., Muñoz-Sabater, J., Nicolas, J., Peubey, C., Radu, R., Schepers, D., Simmons, A., Soci, C., Abdalla, S., Abellan, X., Bal-

samo, G., Bechtold, P., Biavati, G., Bidlot, J., Bonavita, M., De Chiara, G., Dahlgren, P., Dee, D., Diamantakis, M., Dragani, R., Flemming, J., Forbes, R., Fuentes, M., Geer, A., Haimberger, L., Healy, S., Hogan, R. J., Hólm, E., Janisková, M., Keeley, S., Laloyaux, P., Lopez, P., Lupu, C., Radnoti, G., De Rosnay, P., Rozum, I., Vamborg, F., Villaume, S., and Thépaut, J.: The ERA5 global reanalysis, Q. J. Roy. Meteor. Soc., 146, 1999–2049, https://doi.org/10.1002/qj.3803, 2020.

Hille, M. and Den Ouden, J.: Fuel load, humus consumption and humus moisture dynamics in Central European Scots pine stands, Int. J. Wildland Fire, 14, 153, https://doi.org/10.1071/WF04026, 2005.

Hu, Y. and Rein, G.: Development of gas signatures of smouldering peat wildfire from emission factors, Int. J. Wildland Fire, 31, 1014–1032, https://doi.org/10.1071/WF21093, 2022.

Hu, Y., Christensen, E., Restuccia, F., and Rein, G.: Transient gas and particle emissions from smouldering combustion of peat, Proc. Combust. Inst., 37, 4035–4042, https://doi.org/10.1016/j.proci.2018.06.008, 2019.

Huang, X. and Rein, G.: Downward spread of smouldering peat fire: the role of moisture, density and oxygen supply, Int. J. Wildland Fire, 26, 907, https://doi.org/10.1071/WF16198, 2017.

Irannezhad, M., Liu, J., Ahmadi, B., and Chen, D.: The dangers of Arctic zombie wildfires, Science, 369, 1171–1171, https://doi.org/10.1126/science.abe1739, 2020.

Johnston, J., Johnston, L., Wooster, M., Brookes, A., McFayden, C., and Cantin, A.: Satellite Detection Limitations of Sub-Canopy Smouldering Wildfires in the North American Boreal Forest, Fire, 1, 28, https://doi.org/10.3390/fire1020028, 2018.

Jonard, M., Nicolas, M., Coomes, D. A., Caignet, I., Saenger, A., and Ponette, Q.: Forest soils in France are sequestering substantial amounts of carbon, Sci. Total Environ., 574, 616–628, https://doi.org/10.1016/j.scitotenv.2016.09.028, 2017.

Kaiser, J.: GFAS, https://confluence.ecmwf.int/display/CKB/CAMS+global+biomass+burning+emissions+based+on+fire+radiative+power+%28GFAS%29%3A+data+documentation, last access: 22 September 2023.

Kaiser, J. W., Heil, A., Andreae, M. O., Benedetti, A., Chubarova, N., Jones, L., Morcrette, J.-J., Razinger, M., Schultz, M. G., Suttie, M., and van der Werf, G. R.: Biomass burning emissions estimated with a global fire assimilation system based on observed fire radiative power, Biogeosciences, 9, 527–554, https://doi.org/10.5194/bg-9-527-2012, 2012.

Key, C. H. and Benson, N. C.: The normalized burn ratio (NBR): A landsat TM radiometric measure of burn severity, U. S. Geol. Surv. North. Rocky Mt. Sci. Cent. Bozeman, MT, USA, 1999.

Kirkland, M., Atkinson, P. W., Pearce-Higgins, J. W., De Jong, M. C., Dowling, T. P. F., Grummo, D., Critchley, M., and Ashton-Butt, A.: Landscape fires disproportionally affect high conservation value temperate peatlands, meadows, and deciduous forests, but only under low moisture conditions, Sci. Total Environ., 884, 163849, https://doi.org/10.1016/j.scitotenv.2023.163849, 2023.

Kohlenberg, A. J., Turetsky, M. R., Thompson, D. K., Branfireun, B. A., and Mitchell, C. P. J.: Controls on boreal peat combustion and resulting emissions of carbon and mercury, Environ. Res. Lett., 13, 035005, https://doi.org/10.1088/1748-9326/aa9ea8, 2018.

Kopp, O. C.: Coal–Carbon, Organic Matter, Sedimentary Rock, Britannica, https://www.britannica.com/science/coal-fossil-fuel/Structure-and-properties-of-coal, last access: 23 December 2024.

Kreye, J. K., Varner, J. M., Dugaw, C. J., Cao, J., Szecsei, J., and Engber, E. A.: Pine cones facilitate ignition of forest floor duff, Can. J. Forest Res., 43, 512–516, https://doi.org/10.1139/cjfr-2013-0019, 2013.

Krishna, M. P. and Mohan, M.: Litter decomposition in forest ecosystems: a review, Energy Ecol. Environ., 2, 236–249, https://doi.org/10.1007/s40974-017-0064-9, 2017.

Kuklina, V., Sizov, O., Rasputina, E., Bilichenko, I., Krasnoshtanova, N., Bogdanov, V., and Petrov, A. N.: Fires on Ice: Emerging Permafrost Peatlands Fire Regimes in Russia's Subarctic Taiga, Land, 11, 322, https://doi.org/10.3390/land11030322, 2022.

Kurz-Besson, C., Coûteaux, M. M., Berg, B., Remacle, J., Ribeiro, C., Romanyà, J., and Thiéry, J. M.: A climate response function explaining most of the variation of the forest floor needle mass and the needle decomposition in pine forests across Europe, Plant Soil, 285, 97–114, https://doi.org/10.1007/s11104-006-0061-9, 2006.

Laurent, P., Mouillot, F., Yue, C., Ciais, P., Moreno, M. V., and Nogueira, J. M. P.: FRY, a global database of fire patch functional traits derived from space-borne burned area products, Sci. Data, 5, 180132, https://doi.org/10.1038/sdata.2018.132, 2018.

Laurent, P., Mouillot, F., Moreno, M. V., Yue, C., and Ciais, P.: Varying relationships between fire radiative power and fire size at a global scale, Biogeosciences, 16, 275–288, https://doi.org/10.5194/bg-16-275-2019, 2019.

Lee, J. Y., Daube, C., Fortner, E., Ellsworth, N., May, N. W., Tallant, J., Herndon, S., and Pratt, K. A.: Chemical characterization of prescribed burn emissions from a mixed forest in Northern Michigan, Environmental Science Atmospheres, 3, 35–48, https://doi.org/10.1039/D2EA00069E, 2023.

Lelandais, L., Xueref-Remy, I., Riandet, A., Blanc, P. E., Armengaud, A., Oppo, S., Yohia, C., Ramonet, M., and Delmotte, M.: Analysis of 5.5 years of atmospheric CO_2, CH4, CO continuous observations (2014–2020) and their correlations, at the Observatoire de Haute Provence, a station of the ICOS-France national greenhouse gases observation network, Atmos. Environ., 277, 119020, https://doi.org/10.1016/j.atmosenv.2022.119020, 2022.

Lin, S., Liu, Y., and Huang, X.: How to build a firebreak to stop smouldering peat fire: insights from a laboratory-scale study, Int. J. Wildland Fire, 30, 454–461, https://doi.org/10.1071/WF20155, 2021.

Lin, Z., Dai, Y., Mishra, U., Wang, G., Shangguan, W., Zhang, W., and Qin, Z.: On the magnitude and uncertainties of global and regional soil organic carbon: A comparative analysis using multiple estimates, Earth Syst. Sci. Data Discuss. [preprint], https://doi.org/10.5194/essd-2022-232, 2022.

Lopez, M., Schmidt, M., Ramonet, M., Bonne, J.-L., Colomb, A., Kazan, V., Laj, P., and Pichon, J.-M.: Three years of semi-continuous greenhouse gas measurements at the Puy de Dôme station (central France), Atmos. Meas. Tech., 8, 3941–3958, https://doi.org/10.5194/amt-8-3941-2015, 2015.

Loustau, D.: Forests, carbon cycle and climate change, Éd. Quae, Versailles, 2010.

Mack, M. C., Walker, X. J., Johnstone, J. F., Alexander, H. D., Melvin, A. M., Jean, M., and Miller, S. N.: Carbon loss from boreal forest wildfires offset by in-

creased dominance of deciduous trees, Science, 372, 280–283, https://doi.org/10.1126/science.abf3903, 2021.

Madrigal, J., Hernando, C., Guijarro, M., Vega, J. A., Fontúrbel, T., and Pérez-Gorostiaga, P.: Smouldering fire-induced changes in a Mediterranean soil (SE Spain): effects on germination, survival and morphological traits of 3 year-old Pinus pinaster Ait., Plant Ecol., 208, 279–292, https://doi.org/10.1007/s11258-009-9705-1, 2010.

Magro, C., Nunes, L., Gonçalves, O., Neng, N., Nogueira, J., Rego, F., and Vieira, P.: Atmospheric Trends of CO and CH_4 from Extreme Wildfires in Portugal Using Sentinel-5P TROPOMI Level-2 Data, Fire, 4, 25, https://doi.org/10.3390/fire4020025, 2021.

Majdalani, G., Koutsias, N., Faour, G., Adjizian-Gerard, J., and Mouillot, F.: Fire Regime Analysis in Lebanon (2001–2020): Combining Remote Sensing Data in a Scarcely Documented Area, Fire, 5, 141, https://doi.org/10.3390/fire5050141, 2022.

Martin, M., Saby, N., Toutain, B., Chenu, J.-P., Ratié, C., and Boulonne, L.: carbonStocksRegLu.csv, https://doi.org/10.15454/RURZXN/91UG74, 2019.

Masuda, C., Kanno, H., Masaka, K., Morikawa, Y., Suzuki, M., Tada, C., Hayashi, S., and Seiwa, K.: Hardwood mixtures facilitate leaf litter decomposition and soil nitrogen mineralization in conifer plantations, Forest Ecol. Manag., 507, 120006, https://doi.org/10.1016/j.foreco.2021.120006, 2022.

McArthur, A. G. and Cheney, N. P.: The Characterization of Fires in Relation to Ecological Studies, Fire Ecol., 11, 3–9, https://doi.org/10.1007/BF03400629, 2015.

McCarty, J. L., Aalto, J., Paunu, V.-V., Arnold, S. R., Eckhardt, S., Klimont, Z., Fain, J. J., Evangeliou, N., Venäläinen, A., Tchebakova, N. M., Parfenova, E. I., Kupiainen, K., Soja, A. J., Huang, L., and Wilson, S.: Reviews and syntheses: Arctic fire regimes and emissions in the 21st century, Biogeosciences, 18, 5053–5083, https://doi.org/10.5194/bg-18-5053-2021, 2021.

Mebust, A. K., Russell, A. R., Hudman, R. C., Valin, L. C., and Cohen, R. C.: Characterization of wildfire NO_x emissions using MODIS fire radiative power and OMI tropospheric NO_2 columns, Atmos. Chem. Phys., 11, 5839–5851, https://doi.org/10.5194/acp-11-5839-2011, 2011.

Mekonnen, Z. A., Riley, W. J., Randerson, J. T., Shirley, I. A., Bouskill, N. J., and Grant, R. F.: Wildfire exacerbates high-latitude soil carbon losses from climate warming, Environ. Res. Lett., 17, 094037, https://doi.org/10.1088/1748-9326/ac8be6, 2022.

Menut, L., Cholakian, A., Siour, G., Lapere, R., Pennel, R., Mailler, S., and Bessagnet, B.: Impact of Landes forest fires on air quality in France during the 2022 summer, Atmos. Chem. Phys., 23, 7281–7296, https://doi.org/10.5194/acp-23-7281-2023, 2023.

Mickler, R. A., Welch, D. P., and Bailey, A. D.: Carbon Emissions during Wildland Fire on a North American Temperate Peatland, Fire Ecol., 13, 34–57, https://doi.org/10.4996/fireecology.1301034, 2017.

Miyanishi, K. and Johnson, E. A.: Process and patterns of duff consumption in the mixedwood boreal forest, Can. J. Forest Res., 32, 1285–1295, https://doi.org/10.1139/x02-051, 2002.

Moreno-Martínez, Á., Camps-Valls, G., Kattge, J., Robinson, N., Reichstein, M., Van Bodegom, P., Kramer, K., Cornelissen, J. H. C., Reich, P., Bahn, M., Niinemets, Ü., Peñuelas, J., Craine, J. M., Cerabolini, B. E. L., Minden, V., Laughlin, D. C., Sack, L., Allred, B., Baraloto, C., Byun, C., Soudzilovskaia, N. A., and Running, S. W.: A methodology to derive global maps of leaf traits using remote sensing and climate data, Remote Sens. Environ., 218, 69–88, https://doi.org/10.1016/j.rse.2018.09.006, 2018.

Mota, B. and Wooster, M. J.: A new top-down approach for directly estimating biomass burning emissions and fuel consumption rates and totals from geostationary satellite fire radiative power (FRP), Remote Sens. Environ., 206, 45–62, https://doi.org/10.1016/j.rse.2017.12.016, 2018.

Mouillot, F., Schultz, M. G., Yue, C., Cadule, P., Tansey, K., Ciais, P., and Chuvieco, E.: Ten years of global burned area products from spaceborne remote sensing—A review: Analysis of user needs and recommendations for future developments, Int. J. Appl. Earth Obs., 26, 64–79, https://doi.org/10.1016/j.jag.2013.05.014, 2014.

Muller, F.: Strategies for peatland conservation in France – a review of progress, Mires Peat, 21, 1–13, https://doi.org/10.19189/MaP.2016.OMB.218, 2018.

National Centers For Environmental Prediction/National Weather Service/NOAA/U. S. Department Of Commerce: NCEP GFS 0.25 Degree Global Forecast Grids Historical Archive, https://doi.org/10.5065/D65D8PWK, 2015.

Ouest-France: Feux "zombies" à l'origine de la reprise des incendies en Gironde: on vous explique ce phénomène, Ouest-Francefr, https://www.ouest-france.fr/faits-divers/incendie/feux-zombies-a-l-origine-de-la-reprise-des-incendies-en-gironde-on-vous-explique-ce-phenomene-00749e06-1a38-11ed-9b31-1adf573d9c14 (last access: 8 January 2025), 2022.

Parks, S. A.: Mapping day-of-burning with coarse-resolution satellite fire-detection data, Int. J. Wildland Fire, 23, 215, https://doi.org/10.1071/WF13138, 2014.

Pilloix, M.: Inventaire des tourbières françaises et du stock de carbone qu'elles contiennent, 2019.

Prat-Guitart, N., Rein, G., Hadden, R. M., Belcher, C. M., and Yearsley, J. M.: Propagation probability and spread rates of self-sustained smouldering fires under controlled moisture content and bulk density conditions, Int. J. Wildland Fire, 25, 456, https://doi.org/10.1071/WF15103, 2016.

Pribyl, D. W.: A critical review of the conventional SOC to SOM conversion factor, Geoderma, 156, 75–83, https://doi.org/10.1016/j.geoderma.2010.02.003, 2010.

Prichard, S. J., O'Neill, S. M., Eagle, P., Andreu, A. G., Drye, B., Dubowy, J., Urbanski, S., and Strand, T. M.: Wildland fire emission factors in North America: synthesis of existing data, measurement needs and management applications, Int. J. Wildland Fire, 29, 132, https://doi.org/10.1071/WF19066, 2020.

Ramonet, M., Ciais, P., Apadula, F., Bartyzel, J., Bastos, A., Bergamaschi, P., Blanc, P. E., Brunner, D., Caracciolo Di Torchiarolo, L., Calzolari, F., Chen, H., Chmura, L., Colomb, A., Conil, S., Cristofanelli, P., Cuevas, E., Curcoll, R., Delmotte, M., Di Sarra, A., Emmenegger, L., Forster, G., Frumau, A., Gerbig, C., Gheusi, F., Hammer, S., Haszpra, L., Hatakka, J., Hazan, L., Heliasz, M., Henne, S., Hensen, A., Hermansen, O., Keronen, P., Kivi, R., Komínková, K., Kubistin, D., Laurent, O., Laurila, T., Lavric, J. V., Lehner, I., Lehtinen, K. E. J., Leskinen, A., Leuenberger, M., Levin, I., Lindauer, M., Lopez, M., Myhre, C. L., Mammarella, I., Manca, G., Manning, A., Marek, M. V., Marklund, P., Martin, D., Meinhardt, F., Mihalopoulos, N., Mölder, M., Morgui, J. A., Necki, J., O'Doherty, S., O'Dowd, C., Ottosson,

M., Philippon, C., Piacentino, S., Pichon, J. M., Plass-Duelmer, C., Resovsky, A., Rivier, L., Rodó, X., Sha, M. K., Scheeren, H. A., Sferlazzo, D., Spain, T. G., Stanley, K. M., Steinbacher, M., Trisolino, P., Vermeulen, A., Vítková, G., Weyrauch, D., Xueref-Remy, I., Yala, K., and Yver Kwok, C.: The fingerprint of the summer 2018 drought in Europe on ground-based atmospheric CO_2 measurements, Philos. T. R. Soc. B, 375, 20190513, https://doi.org/10.1098/rstb.2019.0513, 2020.

Reddy, A. D., Hawbaker, T. J., Wurster, F., Zhu, Z., Ward, S., Newcomb, D., and Murray, R.: Quantifying soil carbon loss and uncertainty from a peatland wildfire using multi-temporal LiDAR, Remote Sens. Environ., 170, 306–316, https://doi.org/10.1016/j.rse.2015.09.017, 2015.

Rein, G., Cohen, S., and Simeoni, A.: Carbon emissions from smouldering peat in shallow and strong fronts, Proc. Combust. Inst., 32, 2489–2496, https://doi.org/10.1016/j.proci.2008.07.008, 2009.

Rodrigues, M., Cunill Camprubí, À., Balaguer-Romano, R., Coco Megía, C. J., Castañares, F., Ruffault, J., Fernandes, P. M., and Resco de Dios, V.: Drivers and implications of the extreme 2022 wildfire season in Southwest Europe, Sci. Total Environ., 859, 160320, https://doi.org/10.1016/j.scitotenv.2022.160320, 2023.

Roteta, E., Bastarrika, A., Franquesa, M., and Chuvieco, E.: Landsat and Sentinel-2 Based Burned Area Mapping Tools in Google Earth Engine, Remote Sens., 13, 816, https://doi.org/10.3390/rs13040816, 2021.

Rouse, J. W., Hass, R. H., Schell, J. A., Deering, D. W., and Harlan, J. C.: Monitoring the Vernal Advancement and Retrogradation (Greenwave Effect) of Natural Vegetation, NASA/GSFC Type III Final Report, Greenbelt, MD, NASA/GSFC, 1974.

Roy, D. P., Boschetti, L., and Trigg, S. N.: Remote Sensing of Fire Severity: Assessing the Performance of the Normalized Burn Ratio, IEEE Geosci. Remote S., 3, 112–116, https://doi.org/10.1109/LGRS.2005.858485, 2006.

Ruffault, J. and Mouillot, F.: How a new fire-suppression policy can abruptly reshape the fire-weather relationship, Ecosphere, 6, art199, https://doi.org/10.1890/ES15-00182.1, 2015.

Ruffault, J., Curt, T., Moron, V., Trigo, R. M., Mouillot, F., Koutsias, N., Pimont, F., Martin-StPaul, N., Barbero, R., Dupuy, J.-L., Russo, A., and Belhadj-Khedher, C.: Increased likelihood of heat-induced large wildfires in the Mediterranean Basin, Sci. Rep., 10, 13790, https://doi.org/10.1038/s41598-020-70069-z, 2020.

Salis, M., Arca, B., Alcasena, F., Arianoutsou, M., Bacciu, V., Duce, P., Duguy, B., Koutsias, N., Mallinis, G., Mitsopoulos, I., Moreno, J. M., Pérez, J. R., Urbieta, I. R., Xystrakis, F., Zavala, G., and Spano, D.: Predicting wildfire spread and behaviour in Mediterranean landscapes, Int. J. Wildland Fire, 25, 1015, https://doi.org/10.1071/WF15081, 2016.

Scaduto, E., Chen, B., and Jin, Y.: Satellite-Based Fire Progression Mapping: A Comprehensive Assessment for Large Fires in Northern California, IEEE J. Sel. Top. Appl., 13, 5102–5114, https://doi.org/10.1109/JSTARS.2020.3019261, 2020.

Schmidt, M., Lopez, M., Yver Kwok, C., Messager, C., Ramonet, M., Wastine, B., Vuillemin, C., Truong, F., Gal, B., Parmentier, E., Cloué, O., and Ciais, P.: High-precision quasi-continuous atmospheric greenhouse gas measurements at Trainou tower (Orléans forest, France), Atmos. Meas. Tech., 7, 2283–2296, https://doi.org/10.5194/amt-7-2283-2014, 2014.

Scholten, R. C., Jandt, R., Miller, E. A., Rogers, B. M., and Veraverbeke, S.: Overwintering fires in boreal forests, Nature, 593, 399–404, https://doi.org/10.1038/s41586-021-03437-y, 2021.

Schroeder, W., Oliva, P., Giglio, L., and Csiszar, I. A.: The New VIIRS 375 m active fire detection data product: Algorithm description and initial assessment, Remote Sens. Environ., 143, 85–96, https://doi.org/10.1016/j.rse.2013.12.008, 2014.

Schwartz, M., Ciais, P., De Truchis, A., Chave, J., Ottlé, C., Vega, C., Wigneron, J.-P., Nicolas, M., Jouaber, S., Liu, S., Brandt, M., and Fayad, I.: FORMS: Forest Multiple Source height, wood volume, and biomass maps in France at 10 to 30 m resolution based on Sentinel-1, Sentinel-2, and Global Ecosystem Dynamics Investigation (GEDI) data with a deep learning approach, Earth Syst. Sci. Data, 15, 4927–4945, https://doi.org/10.5194/essd-15-4927-2023, 2023.

Sirin, A. and Medvedeva, M.: Remote Sensing Mapping of Peat-Fire-Burnt Areas: Identification among Other Wildfires, Remote Sens., 14, 194, https://doi.org/10.3390/rs14010194, 2022.

Song, Z., Huang, X., Jiang, J., and Pan, X.: A laboratory approach to CO_2 and CO emission factors from underground coal fires, Int. J. Coal Geol., 219, 103382, https://doi.org/10.1016/j.coal.2019.103382, 2020.

Soukissian, T. and Sotiriou, M.-A.: Long-Term Variability of Wind Speed and Direction in the Mediterranean Basin, Wind, 2, 513–534, https://doi.org/10.3390/wind2030028, 2022.

Stein, A. F., Draxler, R. R., Rolph, G. D., Stunder, B. J. B., Cohen, M. D., and Ngan, F.: NOAA's HYSPLIT Atmospheric Transport and Dispersion Modeling System, B. Am. Meteorol. Soc., 96, 2059–2077, https://doi.org/10.1175/BAMS-D-14-00110.1, 2015.

Stracher, G. B. and Taylor, T. P.: Coal fires burning out of control around the world: thermodynamic recipe for environmental catastrophe, Int. J. Coal Geol., 59, 7–17, https://doi.org/10.1016/j.coal.2003.03.002, 2004.

Tang, S., Yin, S., Shan, Y., Yu, B., Cui, C., and Cao, L.: The Characteristics of Gas and Particulate Emissions from Smouldering Combustion in the Pinus pumila Forest of Huzhong National Nature Reserve of the Daxing'an Mountains, Forests, 14, 364, https://doi.org/10.3390/f14020364, 2023.

Tanneberger, F., Tegetmeyer, C., Busse, S., Barthelmes, A., and and 55 others: The peatland map of Europe, Mires Peat, 1–17, https://doi.org/10.19189/MaP.2016.OMB.264, 2017.

Tukey, J. W.: Exploratory data analysis, Vol. 2, 131–160, 1977.

Turetsky, M. R., Donahue, W. F., and Benscoter, B. W.: Experimental drying intensifies burning and carbon losses in a northern peatland, Nat. Commun., 2, 514, https://doi.org/10.1038/ncomms1523, 2011a.

Turetsky, M. R., Kane, E. S., Harden, J. W., Ottmar, R. D., Manies, K. L., Hoy, E., and Kasischke, E. S.: Recent acceleration of biomass burning and carbon losses in Alaskan forests and peatlands, Nat. Geosci., 4, 27–31, https://doi.org/10.1038/ngeo1027, 2011b.

Usman, M., Sitanggang, I. S., and Syaufina, L.: Hotspot Distribution Analyses Based on Peat Characteristics Using Density-based Spatial Clustering, Procedia Environ. Sci., 24, 132–140, https://doi.org/10.1016/j.proenv.2015.03.018, 2015.

Vallet, L. and Mouillot, F.: Carbon Emissions from 2022 fires in France, EasyData [data set], https://doi.org/10.57932/924f1b65-4032-40ce-879d-89a8348ee804, 2025.

Vallet, L., Schwartz, M., Ciais, P., van Wees, D., de Truchis, A., and Mouillot, F.: High-resolution data reveal a surge of biomass loss from temperate and Atlantic pine forests, contextualizing the 2022 fire season distinctiveness in France, Biogeosciences, 20, 3803–3825, https://doi.org/10.5194/bg-20-3803-2023, 2023a.

Vallet, L., Ciais, P., van Wees, D., de Truchis, A., and Mouillot, F.: Forest biomass loss by fire 2020–2022 in France, OSU OREME, https://doi.org/10.15148/3DB37FDF-46B1-4E7A-BD86-CA4FB93307E1, 2023b.

van der Velde, I. R., van der Werf, G. R., Houweling, S., Eskes, H. J., Veefkind, J. P., Borsdorff, T., and Aben, I.: Biomass burning combustion efficiency observed from space using measurements of CO and NO_2 by the TROPOspheric Monitoring Instrument (TROPOMI), Atmos. Chem. Phys., 21, 597–616, https://doi.org/10.5194/acp-21-597-2021, 2021.

van der Werf, G. R., Randerson, J. T., Giglio, L., van Leeuwen, T. T., Chen, Y., Rogers, B. M., Mu, M., van Marle, M. J. E., Morton, D. C., Collatz, G. J., Yokelson, R. J., and Kasibhatla, P. S.: Global fire emissions estimates during 1997–2016, Earth Syst. Sci. Data, 9, 697–720, https://doi.org/10.5194/essd-9-697-2017, 2017.

van Wees, D., van der Werf, G. R., Randerson, J. T., Rogers, B. M., Chen, Y., Veraverbeke, S., Giglio, L., and Morton, D. C.: Global biomass burning fuel consumption and emissions at 500 m spatial resolution based on the Global Fire Emissions Database (GFED), Geosci. Model Dev., 15, 8411–8437, https://doi.org/10.5194/gmd-15-8411-2022, 2022.

Vanguelova, E. I., Bonifacio, E., De Vos, B., Hoosbeek, M. R., Berger, T. W., Vesterdal, L., Armolaitis, K., Celi, L., Dinca, L., Kjønaas, O. J., Pavlenda, P., Pumpanen, J., Püttsepp, Ü., Reidy, B., Simončič, P., Tobin, B., and Zhiyanski, M.: Sources of errors and uncertainties in the assessment of forest soil carbon stocks at different scales—review and recommendations, Environ. Monit. Assess., 188, 630, https://doi.org/10.1007/s10661-016-5608-5, 2016.

Varner, J. M., Kane, J. M., Kreye, J. K., and Engber, E.: The Flammability of Forest and Woodland Litter: a Synthesis, Current Forestry Reports, 1, 91–99, https://doi.org/10.1007/s40725-015-0012-x, 2015.

Veraverbeke, S., Sedano, F., Hook, S. J., Randerson, J. T., Jin, Y., and Rogers, B. M.: Mapping the daily progression of large wildland fires using MODIS active fire data, Int. J. Wildland Fire, 23, 655, https://doi.org/10.1071/WF13015, 2014.

Veraverbeke, S., Dennison, P., Gitas, I., Hulley, G., Kalashnikova, O., Katagis, T., Kuai, L., Meng, R., Roberts, D., and Stavros, N.: Hyperspectral remote sensing of fire: State-of-the-art and future perspectives, Remote Sens. Environ., 216, 105–121, https://doi.org/10.1016/j.rse.2018.06.020, 2018.

Verger, A., Baret, F., Weiss, M., and Weiss, M.: Near real-time vegetation monitoring at global scale., IEEE J. Sel. Top. Appl., 7, 3473–3481, https://doi.org/10.1109/JSTARS.2014.2328632, 2014.

Vernooij, R., Giongo, M., Borges, M. A., Costa, M. M., Barradas, A. C. S., and van der Werf, G. R.: Intraseasonal variability of greenhouse gas emission factors from biomass burning in the Brazilian Cerrado, Biogeosciences, 18, 1375–1393, https://doi.org/10.5194/bg-18-1375-2021, 2021.

Vernooij, R., Winiger, P., Wooster, M., Strydom, T., Poulain, L., Dusek, U., Grosvenor, M., Roberts, G. J., Schutgens, N., and van der Werf, G. R.: A quadcopter unmanned aerial system (UAS)-based methodology for measuring biomass burning emission factors, Atmos. Meas. Tech., 15, 4271–4294, https://doi.org/10.5194/amt-15-4271-2022, 2022.

Walker, X. J., Rogers, B. M., Veraverbeke, S., Johnstone, J. F., Baltzer, J. L., Barrett, K., Bourgeau-Chavez, L., Day, N. J., De Groot, W. J., Dieleman, C. M., Goetz, S., Hoy, E., Jenkins, L. K., Kane, E. S., Parisien, M.-A., Potter, S., Schuur, E. A. G., Turetsky, M., Whitman, E., and Mack, M. C.: Fuel availability not fire weather controls boreal wildfire severity and carbon emissions, Nat. Clim. Change, 10, 1130–1136, https://doi.org/10.1038/s41558-020-00920-8, 2020.

Watts, A. C. and Kobziar, L. N.: Smoldering Combustion and Ground Fires: Ecological Effects and Multi-Scale Significance, Fire Ecol., 9, 124–132, https://doi.org/10.4996/fireecology.0901124, 2013.

Wiedinmyer, C., Kimura, Y., McDonald-Buller, E. C., Emmons, L. K., Buchholz, R. R., Tang, W., Seto, K., Joseph, M. B., Barsanti, K. C., Carlton, A. G., and Yokelson, R.: The Fire Inventory from NCAR version 2.5: an updated global fire emissions model for climate and chemistry applications, EGUsphere [preprint], https://doi.org/10.5194/egusphere-2023-124, 2023.

Wiggins, E. B., Andrews, A., Sweeney, C., Miller, J. B., Miller, C. E., Veraverbeke, S., Commane, R., Wofsy, S., Henderson, J. M., and Randerson, J. T.: Boreal forest fire CO and CH_4 emission factors derived from tower observations in Alaska during the extreme fire season of 2015, Atmos. Chem. Phys., 21, 8557–8574, https://doi.org/10.5194/acp-21-8557-2021, 2021.

Wikipédia: Liste des bassins houillers français, https://fr.wikipedia.org/wiki/Liste_des_bassins_houillers_fran\c{c}ais (last access: 18 October 2023), 2023.

Wooster, M. J., Roberts, G., Perry, G. L. W., and Kaufman, Y. J.: Retrieval of biomass combustion rates and totals from fire radiative power observations: FRP derivation and calibration relationships between biomass consumption and fire radiative energy release, J. Geophys. Res., 110, D24311, https://doi.org/10.1029/2005JD006318, 2005.

Wooster, M. J., Freeborn, P. H., Archibald, S., Oppenheimer, C., Roberts, G. J., Smith, T. E. L., Govender, N., Burton, M., and Palumbo, I.: Field determination of biomass burning emission ratios and factors via open-path FTIR spectroscopy and fire radiative power assessment: headfire, backfire and residual smouldering combustion in African savannahs, Atmos. Chem. Phys., 11, 11591–11615, https://doi.org/10.5194/acp-11-11591-2011, 2011.

Wooster, M. J., Roberts, G. J., Giglio, L., Roy, D. P., Freeborn, P. H., Boschetti, L., Justice, C., Ichoku, C., Schroeder, W., Davies, D., Smith, A. M. S., Setzer, A., Csiszar, I., Strydom, T., Frost, P., Zhang, T., Xu, W., De Jong, M. C., Johnston, J. M., Ellison, L., Vadrevu, K., Sparks, A. M., Nguyen, H., McCarty, J., Tanpipat, V., Schmidt, C., and San-Miguel-Ayanz, J.: Satellite remote sensing of active fires: History and current status, applications and future requirements, Remote Sens. Environ., 267, 112694, https://doi.org/10.1016/j.rse.2021.112694, 2021.

Wu, M., Knorr, W., Thonicke, K., Schurgers, G., Camia, A., and Arneth, A.: Sensitivity of burned area in Europe to climate change, atmospheric CO_2 levels, and demography: A comparison of two fire-vegetation models, J. Geophys. Res.-Biogeo., 120, 2256–2272, https://doi.org/10.1002/2015JG003036, 2015.

Xiang, D., Wang, G., Tian, J., and Li, W.: Global patterns and edaphic-climatic controls of soil carbon decomposition kinetics predicted from incubation experiments, Nat. Commun., 14, 2171, https://doi.org/10.1038/s41467-023-37900-3, 2023.

Xifré-Salvadó, M. À., Prat-Guitart, N., Francos, M., Úbeda, X., and Castellnou, M.: Smouldering Combustion Dynamics of a Soil from a Pinus halepensis Mill. Forest. A Case Study of the Rocallaura Fires in Northeastern Spain, Appl. Sci., 10, 3449, https://doi.org/10.3390/app10103449, 2020.

Yigini, Y. and Panagos, P.: Assessment of soil organic carbon stocks under future climate and land cover changes in Europe, Sci. Total Environ., 557–558, 838–850, https://doi.org/10.1016/j.scitotenv.2016.03.085, 2016.

Yilmaz, O. S., Acar, U., Sanli, F. B., Gulgen, F., and Ates, A. M.: Mapping burn severity and monitoring CO content in Türkiye's 2021 Wildfires, using Sentinel-2 and Sentinel-5P satellite data on the GEE platform, Earth Sci. Inform., 16, 221–240, https://doi.org/10.1007/s12145-023-00933-9, 2023.

Yokelson, R. J., Griffith, D. W. T., and Ward, D. E.: Open-path Fourier transform infrared studies of large-scale laboratory biomass fires, J. Geophys. Res.-Atmos., 101, 21067–21080, https://doi.org/10.1029/96JD01800, 1996.

Zheng, B., Chevallier, F., Ciais, P., Yin, Y., and Wang, Y.: On the Role of the Flaming to Smoldering Transition in the Seasonal Cycle of African Fire Emissions, Geophys. Res. Lett., 45, 11998–12007, https://doi.org/10.1029/2018GL079092, 2018.

Zhou, D. K., Larar, A. M., Liu, X., and Xiong, X.: Estimation of fire-induced CO plume age from NAST–I during the FIREX-AQ field campaign, J. Appl. Remote Sens., 16, 034522, https://doi.org/10.1117/1.JRS.16.034522, 2022.

Zin, E., Kuberski, Ł., Drobyshev, I., and Niklasson, M.: First Spatial Reconstruction of Past Fires in Temperate Europe Suggests Large Variability of Fire Sizes and an Important Role of Human-Related Ignitions, Front. Ecol. Evol., 10, 768464, https://doi.org/10.3389/fevo.2022.768464, 2022.